IVYSPRING INTERNATIONAL PUBLISHER

International Journal of Biological Sciences

2027; 23(1): 612-639. doi: 10.7150/ijbs.142721

Review

Metabolic Geography of Tumor Immunity: How Spatial Metabolic Territories Shape Immune-Cell Fate and Therapeutic Resistance

Xin Yu[1,2,†], Wenge Li[3,†], Qi Wu[4,5]✉, Juanjuan Li[1]✉

1. Department of Breast and Thyroid Surgery, Renmin Hospital of Wuhan University, Wuhan 430060, Hubei, China.
2. Department of Breast Surgery, Fujian Provincial Hospital, Shengli Clinical Medical College of Fujian Medical University, Fuzhou University Affiliated Provincial Hospital, Fuzhou 350001, Fujian, China.
3. Department of Oncology, Fujian Medical University Clinical Teaching Hospital, Fuzhou Pulmonary Hospital of Fujian, Fuzhou 350008, Fujian, China.
4. Zhejiang Provincial Key Laboratory of Pancreatic Disease, Hangzhou 310016, Zhejiang, China.
5. Department of Hepatobiliary and Pancreatic Surgery, The First Affiliated Hospital, Zhejiang University School of Medicine, Hangzhou 311121, Zhejiang, China.

†These authors have contributed equally to this work and share first authorship.

✉ Corresponding authors: Dr. Juanjuan Li, Department of Breast and Thyroid Surgery, Renmin Hospital of Wuhan University, Wuhan 430060, Hubei, China. E-mail: juanjuan.li@whu.edu.cn. Dr. Qi Wu, Department of Hepatobiliary and Pancreatic Surgery, The First Affiliated Hospital, Zhejiang University School of Medicine, Hangzhou 311121, Zhejiang, China. E-mail: waiwai@whu.edu.cn.

© 2027 The Author(s). This is an open access article distributed under the Creative Commons Attribution 4.0 International Licence, subject to the Publisher's Terms of Use at https://ivyspring.com/terms.

Received: 2026.08.18; Accepted: 2026.10.26; Published: 2027.01.01

Abstract

Metabolic regulation of antitumor immunity varies across the tumor microenvironment. Differences in perfusion, tissue architecture, cellular demand and metabolite clearance create local conditions that influence immune-cell entry, activation, differentiation and persistence. This review examines spatial metabolic territories by distinguishing measurable physicochemical fields from multicellular niches and anatomical contexts. It relates metabolic sources and recipients to exposure duration, functional recovery and regional treatment resistance. It further considers how the effects of metabolic factors vary with local chemical conditions, cellular state, exposure history and the intervention examined. Spatial transcriptomics and protein imaging characterize cellular organization and support inference of metabolic capacity, whereas metabolite measurements, physiological sensors, isotope tracing and selective perturbations address different aspects of mechanism. Human evidence remains uneven, especially for nutrient support within tertiary lymphoid structures and endogenous intercellular transfer. Clinical trial evidence from metabolic-pathway interventions illustrates the distinction between pathway activity and validation of a spatial predictive biomarker. Linking reproducible tissue features to direct measurements and prospective treatment outcomes may help identify regional barriers while preserving the immune niches required for durable antitumor responses.

Keywords: tumor immunometabolism; spatial metabolomics; spatial metabolic heterogeneity; tumor microenvironment; immune-cell fate; therapeutic resistance

1. Introduction

Metabolic reprogramming and immune evasion are closely interconnected features of cancer biology[1, 2]. Activated lymphocytes, myeloid cells, fibroblasts and malignant cells remodel nutrient uptake and biosynthesis under different functional constraints. Effector differentiation, memory formation and regulatory activity involve overlapping but context-dependent metabolic programs[3, 4]. The tumor microenvironment (TME) is therefore not simply nutrient poor: nutrients, metabolic by-products and stress signals are continuously exchanged among malignant, stromal and immune populations. These interactions can restrict checkpoint blockade, cellular therapy and the formation of durable immune memory[5].

Bulk tissue and dissociated-cell measurements have established many metabolic dependencies but obscure their local organization. Solid tumors exhibit

variability in perfusion, diffusion distance, extracellular-matrix density, cell composition and waste clearance. A glycolytic signature does not reveal whether glucose is locally available, which population exports lactate or which neighboring cells consume it. Cell-resolved tracer studies show that myeloid cells can display the greatest glucose uptake while malignant cells preferentially acquire glutamine[6]. Quantification of tumor interstitial fluid in mouse models likewise shows that nutrient availability differs from plasma and varies with tumor type, anatomical site and diet[7]. Together, these findings make substrate availability and recipient identity necessary components of a regional comparison.

Recent reviews have established spatial immunometabolism as a field and described its analytical technologies, while broader analyses have placed metabolic heterogeneity within tumor progression and treatment adaptation[8, 9]. Here, metabolic geography is used as an operational framework linking a metabolic source, a susceptible recipient and the conditions of their interaction. Distance and tissue transport shape exposure, while exposure duration and the recipient's differentiation state influence subsequent recovery. Local immune organization can affect access and renewal without establishing a corresponding nutrient advantage[8, 9]. The framework centers on which population produces or consumes a factor, which recipient encounters it, how exposure affects recovery, and whether spatial organization adds information beyond cell density, tissue composition and bulk metabolism.

2. Spatial organization of metabolic heterogeneity in the tumor microenvironment

A spatial metabolic territory is a tumor region characterized by a specified metabolic or physicochemical property at a stated spatial scale and time. Its description should identify the measured variable and compartment, the method used to delimit the region, relevant source and recipient populations, and the immune outcome under study. A region defined only by enzyme or transporter expression is a candidate metabolic territory until the relevant chemistry or physiology is measured. The appropriate scale follows the interaction: cell contact, a multicellular neighborhood, a tissue region and an entire lesion answer different questions. Analyses should report distances in physical units, effective resolution and registration error, and test whether findings persist across reasonable neighborhood definitions (Table 1). Spatial localization, direct metabolic measurement, cell-specific perturbation and human clinical association provide different forms of support and need not occur together in the same study (Table 2). Intercellular routes such as organelle transfer describe mechanisms that may operate within a territory; they do not define its boundaries.

Table 1. Operational definitions and reporting requirements for spatial metabolic analysis

Term	Operational meaning	Minimum measurement or reporting information
Metabolic territory	A region characterized by a specified metabolic or physicochemical property at a stated scale and time. Expression-only maps define candidates.	Variable, units, intracellular/extracellular compartment, platform, effective resolution, boundary rule, time point, source and recipient, and immune endpoint. Avoid assigning a measured field to an entire cellular niche without chemical evidence.
Field	A continuously varying chemical or physiological property, such as oxygen, pH or lactate.	Calibration, sampling density, dynamic range, uncertainty and whether the field was measured in vivo or after excision. Tissue metabolite abundance may combine several cellular and extracellular pools.
Niche	A recurrent cellular arrangement associated with a local function.	Cell identities, architecture, neighborhood rule and functional association. A TLS or APC–T cell hub can be defined structurally; metabolic support requires an additional measurement.
Region and compartment	Region denotes the analyzed tissue area; compartment denotes an anatomical or biophysical division.	Region boundaries, viable and necrotic fractions, anatomical site and the compartment actually sampled. Intracellular signal cannot automatically be interpreted as extracellular exposure.
Spatial scale	The interaction scale appropriate to the biological question, from cell contact to neighborhood, tissue region or lesion.	Distances in micrometers or millimeters, section thickness, effective resolution, registration error and sensitivity to neighborhood size. The framework has no universal distance threshold.
Exposure history	The trajectory of a recipient's exposure, including concentration, duration, repetition and order.	Controlled protocols or calibrated live recordings can measure a trajectory. Serial samples describe population-level intervals. Endpoint RNA/chromatin signatures are labeled exposure proxies; they do not uniquely recover a cell's prior chemistry.
Functional recovery	Return of a prespecified function after removal of a specified stress under defined conditions.	Washout, residual exposure, nutrients, pH, oxygen, cytokines, antigen stimulus and recovery time. Include unexposed, continuously exposed and recovery groups, matched viability and functional endpoints. Example times of 0, 24 and 72 h require pilot adaptation; there is no universal recovery schedule.
Target engagement	Evidence that the intervention reaches and modulates its intended target in the relevant cells or region.	Regional exposure plus an appropriate occupancy, enzymatic, transport or pathway assay. A downstream concentration change alone may have several causes; immune benefit is assessed separately.
Metabolic niche substitution	A different metabolic process maintains local dysfunction after the original suppressive process is inhibited.	Original-target engagement, comparable longitudinal regions, candidate alternative chemistry and functional rescue after its perturbation. Distinguish inadequate delivery, clonal or compositional selection and unmeasured tissue from substitution.

These definitions specify how a study can be interpreted; they are not validated clinical cutoffs or a universal assay protocol. Source, exposure and recipient measurements can come from complementary platforms, with uncertainty and compartment differences retained. APC, antigen-presenting cell; TLS, tertiary lymphoid structure.

Table 2. Evidence for physicochemical fields, cellular niches and intercellular metabolic mechanisms

Entity and defining feature	Representative study and material	Spatial or metabolic measurement	Model perturbation and human observations	Unresolved measurement
Physicochemical fields and exposure conditions				
Hypoxic field Locally reduced oxygen availability	Chronic ATF4 activity in patient TILs and tumor models[25]	Patient stress-state observations; experimental hypoxic exposure and metabolic dysfunction. ATF4 is not a calibrated oxygen readout.	Model perturbation: ISR attenuation improved T cell viability and PD-1 response. Human observations: ATF4-associated TIL stress states.	Cell-resolved oxygen exposure, duration and recovery in human tumors.
Acidic field Reduced extracellular pH	Acid-conditioned T cells; SLC4A4 in pancreatic cancer[33, 34]	Controlled acidosis and biochemical studies; tumor pH regulation in experimental systems.	Model perturbation: acidic conditioning preserved later persistence; SLC4A4 inhibition improved pancreatic tumor immunity. Human observations: no validated local pH response threshold.	Joint local pH, lactate and cell-state measurements; a clinically validated response threshold.
Peri-necrotic adenosine Localized purine enrichment	Graziano and colleagues; mouse pancreatic tumors and human expression datasets[26]	MSI adenosine localization registered to hypoxic, myeloid-rich regions in mice.	Model perturbation: CD73/A2AR blockade improved treatment activity. Human observations: expression signature–outcome association.	Direct extracellular concentration and recipient exposure in patient tissue.
Ionic field Elevated extracellular potassium	Potassium perturbation and human liver/colorectal tumor profiling[38, 39]	Controlled potassium exposure; spatial cell phenotypes in necrosis-prone human regions.	Model perturbation: potassium altered effector activity and differentiation. Human observations: spatial phenotypes in necrosis-prone regions.	Matched in situ potassium, osmolarity and individual-cell exposure history.
Lactate-associated conditions Lactate and pH recorded separately	MCT11, Treg MCT1, sodium lactate and lactic acid studies[43, 44, 45, 46, 48]	Transport and metabolic assays under different chemical and differentiation conditions.	Model perturbation: transporter interventions and controlled exposures produced distinct immune effects. Human observations: no joint lactate/pH/uptake/function map in the studies compared.	A common human region with paired lactate, pH, uptake and functional measurements.
Lipid/oxidative conditions Species, uptake and damage specified	CD36-associated T cell dysfunction and NK-cell lipotoxicity[53, 54, 144]	Cell-specific lipid uptake, peroxidation and metabolic assays; tumor or obesity models.	Model perturbation: uptake and lipid-handling interventions support cytotoxic-cell impairment. Human observations: no complete regional exposure map in the studies compared.	Regional lipid species, source attribution and recipient-specific oxidative injury.
Cellular niches and interfaces				
Perivascular/APC–T cell niche Cellular organization and renewal	HEV remodeling; human APC niches and immune hubs[85, 86, 87, 88]	Cellular location, differentiation and clinical association; experimental endothelial remodeling.	Model perturbation: endothelial remodeling supported entry and renewal. Human observations: APC niches, clonal differentiation and response-associated hubs.	Local oxygen, amino-acid and lactate supply and flux within the niche.
TLS Mature B/T-cell and stromal architecture	Melanoma, head-and-neck and lung cancer studies[99, 100, 102, 105]	Structural and transcriptional organization; ACAT1-related experimental niche regulation.	Model perturbation: ACAT1-related regulation of TLS formation. Human observations: TLS organization, abundance and outcome associations.	Whether a directly measured metabolic feature is required for local priming or persistence.
GLUT1-positive TAM interface TAM–CD8 spatial segregation	Non-small-cell lung cancer specimens and mouse tumors[91]	Human spatial association; transporter-positive TAM localization.	Model perturbation: TAM-specific SLC2A1 deletion improved T cell distribution/function. Human observations: TAM–CD8 segregation and treatment resistance.	Magnitude and direction of local glucose redistribution; segregation itself is not causal proof.
CAF-rich interface Stromal state and boundary defined	Sarcoma glyCAF and oral cancer spatial transcriptomics[23, 96]	Spatial stromal/transcriptional patterns; glycolytic CAF perturbation in sarcoma.	Model perturbation: glycolytic CAF targeting reduced sarcoma T cell exclusion. Human observations: oral cancer spatial expression patterns; lactate exchange inferred.	Direct epithelial-to-CAF transfer and separation of matrix, chemokine and metabolic effects.
Intercellular resource interactions, transfer and signaling				
Methionine competition Tumor-to-T-cell resource interaction	Tumor SLC43A2 and T cell methylation[68]	Biochemical nutrient competition and T cell methyl-donor/histone measurements.	Model perturbation: tumor SLC43A2 targeting altered T cell methylation and function. Human observations: molecular/functional support, without adjacent-cell flux quantification.	Direct adjacent-cell flux and quantitative human extracellular gradients.
Glutamine acquisition and antagonism Recipient-specific dependencies	cDC1 SLC38A2 and glutamine-antagonist studies[71, 72]	Glutamine uptake/sensing and metabolic adaptation in experimental systems.	Model perturbation: SLC38A2–FLCN/TFEB dependence in cDC1s; divergent effector T cell adaptation to JHU083. Human observations: regional recipient dependence unresolved.	Which recipient limits benefit within a specific patient region.
Tumor mitochondrial transfer Organelle entry into T cells	Patient tumor/TIL mtDNA variants and transfer models[19]	Shared variants in clinical samples; experimental transfer and persistence.	Model perturbation: transferred mitochondria induced metabolic defects, senescence and impaired immunity. Human observations: shared tumor/TIL mtDNA variants and prognostic association.	Endogenous direction, frequency and complete trajectory at single-cell resolution in patients.
NAMPT-containing vesicles Macrophage-to-CAF influence	Gastric cancer patient observations and functional systems[20]	Transcriptomic/plasma observations and vesicle-mediated nicotinamide pathway studies.	Model perturbation: NAMPT vesicles suppressed CAF NNMT through SIRT1/NICD; vesicle administration restored CD8 and anti-PD-1 activity. Human observations: transcriptomic and serial plasma associations.	Endogenous human vesicle origin, cargo association and recipient uptake.
Extracellular GPX4 signaling GPX4 binding to DC ZP3	Preclinical ferroptosis studies and clinical associations[21]	Released GPX4, surface-receptor interaction and DC metabolic response.	Model perturbation: GPX4–ZP3 blockade restored DC activity. Human observations: circulating GPX4/DC ZP3 associated with resistance.	Causal local receptor engagement in human tumors; vesicle uptake is not required.

Physicochemical fields/exposure conditions and cellular niches/interfaces describe spatial properties or cellular arrangements; intercellular resource interactions, transfer and signaling describe mechanisms that may operate within them, not additional territories. For transparency, Table 2 distinguishes three evidence dimensions without converting them into an ordinal score: direct chemical or physiological measurement, preclinical causal support from selective experimental perturbation linked to function, and human associative or spatial evidence without causal intervention. A causal model result does not establish the same metabolic field in patients, and spatial association is not equivalent to causal perturbation. Unmeasured does not mean absent. A2AR, adenosine A2A receptor; APC, antigen-presenting cell; ATF4, activating transcription factor 4; CAF, cancer-associated fibroblast; cDC1, conventional type 1 dendritic cell; DC, dendritic cell; FLCN, folliculin; GPX4, glutathione peroxidase 4; HEV, high

endothelial venule; ISR, integrated stress response; MCT, monocarboxylate transporter; MSI, mass spectrometry imaging; mtDNA, mitochondrial DNA; NAMPT, nicotinamide phosphoribosyltransferase; NICD, Notch intracellular domain; NK, natural killer cell; NNMT, nicotinamide N-methyltransferase; SIRT1, sirtuin 1; TAM, tumor-associated macrophage; TFEB, transcription factor EB; TIL, tumor-infiltrating lymphocyte; TLS, tertiary lymphoid structure; Treg, regulatory T cell; ZP3, zona pellucida glycoprotein 3.

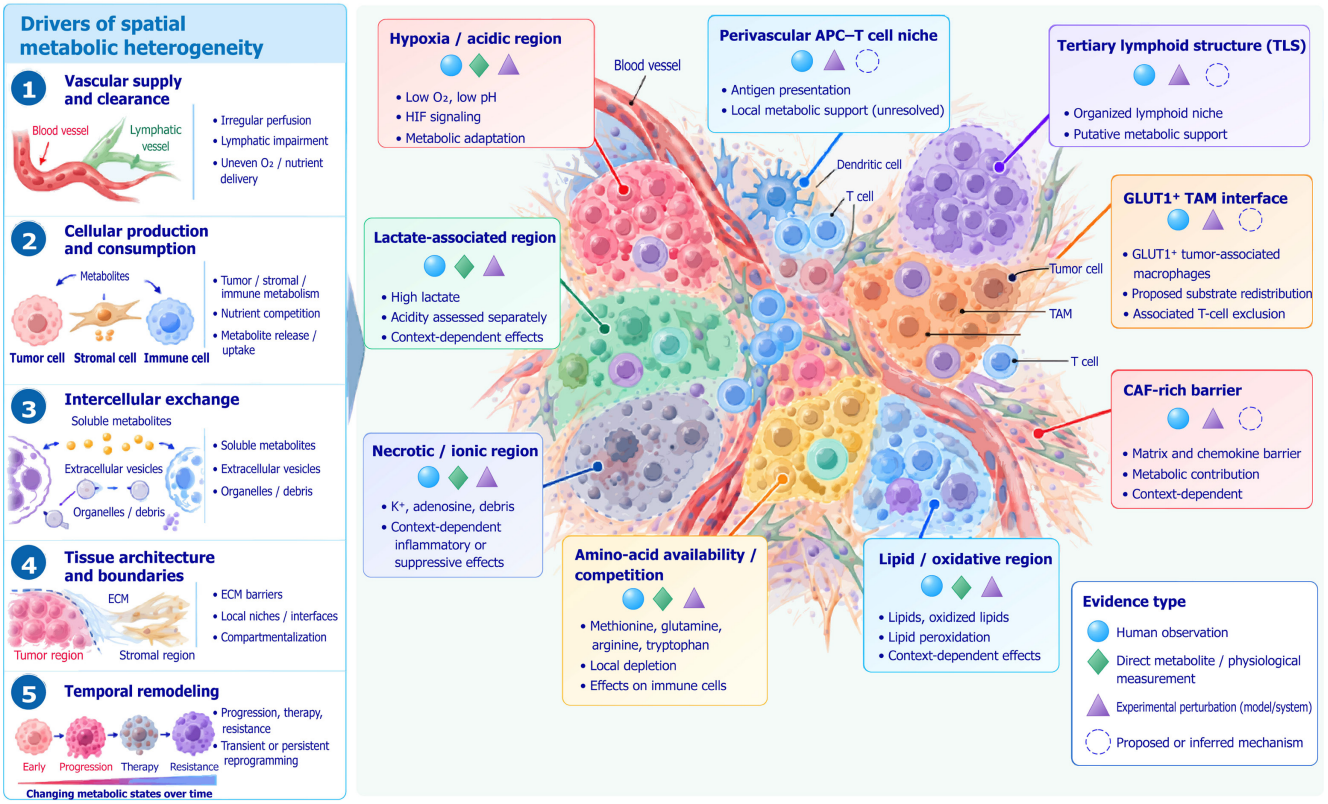

Figure 1. Drivers and spatial manifestations of metabolic heterogeneity in the tumor microenvironment. Vascular supply and clearance, cellular production and consumption, intercellular exchange, tissue architecture and boundaries, and temporal remodeling generate overlapping spatial metabolic patterns. Representative manifestations include hypoxic/acidic, lactate-associated, necrotic/ionic, amino-acid availability/competition and lipid/oxidative regions, together with perivascular APC–T-cell niches, TLS, GLUT1-positive TAM interfaces and CAF-rich barriers. Their schematic positions imply neither fixed compartments nor hierarchical order. Local metabolic support within APC–T-cell niches remains unresolved, metabolic support within TLS is putative, and substrate redistribution at GLUT1-positive TAM interfaces remains a proposed explanation. Associated T-cell exclusion does not itself establish direct local glucose competition. Lactate abundance and acidity are considered separately. Blue circles indicate human observations, which may be spatial or non-spatial; green diamonds indicate direct metabolic or physiological measurements; purple triangles indicate experimental perturbation; and dashed circles indicate proposed or inferred mechanisms. Symbols identify evidence types represented in the relevant literature rather than support for every statement within a box, a unified evidence score, or proof that all measurements were obtained in the same study or patient region. Direct measurements may derive from experimental systems and do not automatically establish human extracellular concentrations or flux. Table 2 specifies study material, spatial evidence and unresolved measurements. APC, antigen-presenting cell; CAF, cancer-associated fibroblast; ECM, extracellular matrix; GLUT1, glucose transporter 1; HIF, hypoxia-inducible factor; TAM, tumor-associated macrophage; TLS, tertiary lymphoid structure.

A field denotes a continuously varying property such as oxygen tension, pH or lactate concentration. A niche denotes a recurrent cellular arrangement associated with a local function, such as an antigen-presenting-cell (APC)–T cell hub. Region is a neutral term for a sampled or analyzed area, whereas compartment refers to an anatomical or biophysical division, including intracellular and extracellular spaces. Fields and niches can overlap without sharing boundaries: a tertiary lymphoid structure (TLS) is defined by cellular architecture, and its presence does not establish a nutrient-rich territory. Vascular supply, production, consumption and transport generate heterogeneity; tissue organization and organ site modify its expression; time affects all of these relationships[8, 9] (Figure 1).

2.1 Vascular supply, cellular demand and tissue transport

Abnormal tumor vessels are irregular, permeable and incompletely supported by pericytes. Heterogeneous flow creates neighboring regions with continuous, intermittent or negligible oxygen and nutrient delivery. Elevated interstitial pressure and impaired drainage further limit transport and waste clearance. Perfusion therefore influences glucose, amino-acid and lipid supply, the removal of protons and lactate, and the penetration of antibodies or small molecules[10, 11]. Distance to a vessel is an incomplete surrogate because vessels may be compressed, shunted or poorly oxygenated. Integrated imaging, respirometry and ultrastructural analysis in lung cancer identified distinct mitochondrial organization

and bioenergetic phenotypes, illustrating metabolic variation that bulk assays can obscure[12]. Such variation need not follow a smooth gradient from a perfused rim to a necrotic core.

Endothelial cells also regulate the supply interface. In preclinical liver cancer, tumor-derived cyclic GMP–AMP activates endothelial stimulator of interferon genes (STING) signaling and promotes vascular normalization and lymphocyte recruitment[13]. In glioblastoma, endothelial phosphoglycerate dehydrogenase (PHGDH)-dependent serine metabolism contributes to abnormal vascular growth, hypoxia and resistance to chimeric antigen receptor T cell (CAR-T) therapy in models informed by human and mouse tumors[14]. Vessel number alone consequently cannot capture the metabolic or immunological effects of vascular intervention. Perfusion and endothelial state must be considered alongside the organization of downstream tissue.

Production, consumption and transmembrane transport are coupled components of local metabolism. Cell density, activation, proliferation and downstream pathway activity influence which substrates are retained or released. Glucose transporter 1 (GLUT1; encoded by SLC2A1), monocarboxylate transporters 1 and 4 (MCT1 and MCT4), CD36 and amino-acid carriers indicate uptake or export capacity, but expression does not determine net flux independently of substrate gradients and intracellular demand[6, 7]. A high tissue concentration can reflect high production, slow consumption or poor clearance. Spatial flux balance analysis (spFBA) predicts lactate-consuming regions in colorectal primary tumors and liver metastases and heterogeneous lactate-producing regions in renal cancer; these are model-derived patterns rather than direct measurements of exchange[15].

Cell identity can be as important as malignant-cell abundance. Spatial metabolomics found lower itaconate levels in lung tumor regions than in adjacent tissue, while macrophage immune-responsive gene 1 (IRG1, also termed ACOD1)-dependent itaconate limited tumor growth and altered glucose metabolism in experimental systems[16]. Chemotherapy-associated lipid oxidation in a PTGER3-positive cancer-associated fibroblast (CAF) subset supported $CD8^+$ T cell activity rather than uniformly suppressing it[17]. Obesity-induced programmed cell death protein 1 (PD-1) expression on macrophages, by contrast, impaired their glycolysis, phagocytosis and T cell stimulatory function[18]. These examples caution against assigning a fixed immune effect to a lineage or pathway. Organelles, vesicle-associated enzymes and extracellular proteins add forms of intercellular influence beyond freely diffusible metabolites[19, 20, 21].

Tissue structure sets the distances over which these processes interact. Collagen-rich stroma and contractile fibroblasts can compress vessels and impede lymphocyte movement[10, 11], while spatial CAF neighborhoods differ in cellular composition and immune association[22]. In soft-tissue sarcoma models, a glycolytic CAF population used GLUT1-dependent CXCL16 expression to restrict T cell infiltration, linking a stromal metabolic dependency to a chemotactic barrier[23]. A boundary may therefore combine structural, signaling and metabolic effects. The presence of one does not prove the others, and reducing a metabolic program may leave a physical barrier intact.

2.2 Physicochemical fields

Oxygen tension, pH, ion composition and metabolite abundance vary with supply, consumption and clearance[8, 9, 10, 11]. These variables define overlapping fields rather than fixed anatomical compartments, and their immune consequences depend on the chemical species, responding cell and exposure conditions[5, 8, 9]. Table 2 distinguishes the measurements and functional evidence available for representative fields.

2.2.1 Hypoxia, acidity and purinergic signaling

Poor perfusion can combine oxygen limitation, acidosis and impaired waste clearance, although these features should be measured separately[24]. Sustained activating transcription factor 4 (ATF4) activity was detected in patient $CD8^+$ tumor-infiltrating lymphocytes (TILs). Experimental studies showed that hypoxia-driven integrated stress response (ISR) signaling caused mitochondrial oxidative stress, loss of viability and an exhaustion-like transcriptional state, while genetic or pharmacological attenuation improved responses to PD-1 inhibition[25]. This supports a stress-dependent immune mechanism without making ATF4 expression a quantitative oxygen measurement. In mouse pancreatic cancer, mass spectrometry imaging (MSI) localized adenosine enrichment to hypoxic, myeloid-rich peri-necrotic regions. Combined CD73 and adenosine A2A receptor (A2AR) inhibition reduced suppressive immune populations and improved treatment activity[26]. Human transcriptomic associations in that study complemented the experimental evidence but did not directly establish the same extracellular concentration map in patients.

Different cells interpret hypoxia through distinct pathways. Hypoxia can induce CD39-dependent suppressive activity in exhausted T cells[27], early

growth response 1 (EGR1)-dependent neutrophil remodeling[28], and histone lactylation associated with neutrophil-mediated T cell suppression in brain tumors[29]. Tumor-derived lipocalin 2 links ISR activity to immune evasion[30], whereas La-related protein 4 (LARP4)-dependent hypertranslation and mitochondrial dysfunction contribute to T cell failure through distinct mechanisms[31, 32]. Acidity has similarly context-dependent effects. Prolonged acidic conditioning restricted methionine uptake and one-carbon metabolism while preserving a stem-like memory state and improving subsequent T cell persistence in mice[33]. In pancreatic cancer models, inhibiting the bicarbonate transporter SLC4A4 reduced extracellular acidosis and improved antitumor immunity[34]. These findings concern different cells, exposure histories and functional endpoints; they do not establish a universally favorable pH range.

Endoplasmic reticulum (ER) stress adds another distinction between the malignant and immune compartments[35]. In ovarian cancer, inositol-requiring enzyme 1 alpha (IRE1α)–X-box binding protein 1 (XBP1) signaling impaired T cell mitochondrial respiration by limiting glutamine influx under glucose-restricted conditions[36]. In a separate mechanism, ablation of protein kinase R-like ER kinase (PERK) in malignant cells induced paraptosis and dendritic-cell type I interferon responses that promoted antitumor T cell immunity[37]. These results support cell-specific interpretations of ER stress rather than a common effect of activating or inhibiting the entire pathway.

2.2.2 Necrosis and ionic conditions

Necrosis releases intracellular ions and metabolites into the extracellular space, with potassium providing a well-defined example of an immunoregulatory signal[38]. Elevated extracellular potassium can suppress T cell receptor signaling and effector activity[38]. A later study linked high-potassium exposure to altered glucose and glutamine metabolism and preferential type 2 helper T cell (Th2) and induced regulatory T cell (Treg) differentiation; analogous phenotypes were found in necrosis-prone regions of human liver and colorectal tumors[39]. The patient observations do not by themselves quantify the potassium exposure of each cell. Cell death can promote antigen-dependent immune responses[40], whereas necroptosis-associated signals can sustain immune suppression in experimental tumors[41]. Necrotic area alone therefore cannot distinguish an immunogenic response from chronic suppression. Potassium effects should also be separated from sodium and osmotic effects: controlled sodium chloride exposure enhanced $CD8^+$ T cell effector function in experimental cancer immunotherapy[42]. Ion-specific measurement and controls for counter-ions, pH and osmolarity are needed before culture conditions are extrapolated to tissue.

2.2.3 Lactate and lactylation

Lactate illustrates why chemical conditions and cell state must be considered together. Tumor-associated lactic acid production can inhibit T and natural killer (NK) cell function[43]. Terminally exhausted $CD8^+$ T cells can acquire MCT11-dependent lactate uptake that reinforces dysfunction[44], whereas Tregs use MCT1-mediated lactate uptake to sustain metabolism and increase PD-1 expression in highly glycolytic tumors[45, 46, 47]. Under other experimental conditions, sodium lactate increased T cell factor 1 (TCF-1) expression and stem-like properties of $CD8^+$ T cells[48]. These studies interrogated different exposures and outcomes. For example, the MCT11 study tested a 5-hour lactic acid challenge in previously conditioned exhaustion-like cells, whereas the stemness study examined longer sodium lactate conditioning and subsequent persistence-related endpoints[44, 48]. The selected conditions are compared in Table 3A. The chemical form, dose, measured pH and initial differentiation state must accompany any comparison of the reported immune effects.

Lactate concentration, transporter-dependent uptake, intracellular carbon use and protein lactylation are distinct measurements. LDH inhibition redistributed glucose uptake toward immune cells in mouse tumors[49], whereas lactylation studies identified specific protein or histone modifications associated with suppressive programs in pancreatic cancer and brain-tumor neutrophils[29, 50, 51]. Alanyl-tRNA synthetase 1 (AARS1)-mediated activating transcription factor 6 (ATF6) lactylation also affected tryptophan metabolism and immune evasion in hepatocellular carcinoma[52]. Tissue lactate abundance cannot establish these modifications or their timing. Different recipients may therefore respond differently within a region with similar extracellular lactate, while a single lineage may show acute suppression during exposure and improved persistence after conditioning. Acidosis-mediated preservation of stemness likewise does not imply preserved effector activity during acidic exposure[33].

Table 3. Experimental conditions underlying divergent immune effects of lactate and glutamine interventions

Study and recipient state	Form and dose	Duration and stage	pH and oxygen	Functional endpoints	Reported result	Interpretation for regional comparison
A Lactate exposure and recipient state						
Peralta et al.[44] Murine $CD8^+$ cells conditioned to an exhaustion-like state	Lactic acid, 0 or 5 mM; MCT11 antibody control/intervention	5-h restimulation after continuous stimulation and hypoxic conditioning	Extracellular pH: NR. Conditioning included 1.5% O_2.	TNF/IL-2 production after restimulation; transporter-dependent dysfunction	MCT11 blockade mitigated the additional functional suppression associated with the lactate challenge.	An acute challenge in an already stressed recipient. It cannot establish that every lactate-exposed $CD8^+$ population has the same response.
Watson et al.[46] Activated murine Treg and conventional T cells	Lactic acid, 10 mM; lactate-use and MCT1-related perturbations	3-day conditioning in proliferation and suppression assays	Extracellular pH: NR for the selected assay. Oxygen not an independently matched variable.	Proliferation and suppression of responder T cell proliferation	Tregs maintained lactate-supported activity under conditions restrictive to conventional T cells.	Lineage and metabolic handling alter the outcome. Joint pH, dose and uptake measurements are needed before extrapolating to a shared human region.
Feng et al.[48] Activated murine OT-I and human cord-blood $CD8^+$ cells	Sodium lactate, 40 mM; control medium contained lower lactate	Expansion assessed on day 8; separate 4-day pretreatment before adoptive transfer	pH 7.4 in sodium-lactate medium; acidity comparisons included pH 6.9. Oxygen was not the principal comparison.	TCF-1/CXCR3, apoptosis and subsequent tumor control after transfer	Increased stem-like markers, reduced apoptosis and improved later antitumor activity in the tested systems.	Conditioning and persistence-related outcomes differ from acute effector inhibition. Salt form, osmolarity and pH must accompany the comparison.
B Glutamine availability and pathway antagonism						
Guo et al.[71] In vitro-derived immature DCs with MC38 cells	Glutamine, 2 versus 0.6 mM; Transwell coculture	24-h DC–tumor coculture	Extracellular pH: NR. No independently matched oxygen perturbation in this comparison.	DC CD86 and MHCII expression	Tumor-associated maturation was impaired at the lower glutamine concentration.	Tests resource availability at the antigen-presenting step. Transwell competition supports a soluble influence, without mapping a human intratumoral gradient.
Guo et al.[71] Murine cDC1s with DC-specific SLC38A2/FLCN pathway perturbation	Genetic perturbation: dose NA. Selected uptake assay used 2 mM $^{13}C_5$-glutamine.	Uptake measured over 10 min; priming and tumor-control endpoints used separate functional assays	Extracellular pH: NR for the selected functional comparisons.	Glutamine acquisition, antigen-specific T cell priming and response to supplementation	cDC1 acquisition/sensing was required for effective priming and supplementation-associated benefit.	Recipient-specific loss does not model broad pharmacological antagonism. Uptake kinetics and later priming are distinct readouts.
Leone et al.[72] Tumor cells and established murine $CD8^+$ TILs	JHU083, 0.3 mg/kg/day in the selected TIL-analysis experiment	Treatment on days 14–18 after tumor inoculation; analysis on day 18	No fixed tumor pH; hypoxia/acidity were tumor-context readouts rather than imposed pH strata.	TIL activation, IFN-γ/granzyme B, proliferation, survival and metabolic adaptation	Cancer-cell metabolic programs were suppressed while T cells acquired greater oxidative and persistent effector features.	Broad pathway antagonism and whole-tumor remodeling differ from cDC1 transporter deletion. Drug exposure and immune stage may determine which effect limits outcome.

The table compares selected experiments, not every dose or assay in each publication. Doses are extracellular additions, tracer concentrations or administered drug doses as specified; they are not interchangeable measures of recipient exposure. NR means that a numerical extracellular pH was not specified for the selected experiment; it does not assign a standard culture pH. NA, not applicable. Conditioning and acute challenge intervals are distinguished. Reported stem-like markers do not alone prove long-term renewal; downstream functional results are listed separately. cDC1, conventional type 1 dendritic cell; DC, dendritic cell; FLCN, folliculin; IFN-γ, interferon gamma; IL-2, interleukin 2; MCT, monocarboxylate transporter; MHCII, major histocompatibility complex class II; TCF-1, T cell factor 1; TIL, tumor-infiltrating lymphocyte; TNF, tumor necrosis factor; Treg, regulatory T cell.

Contrasting effects reported after lactic-acid exposure, sodium-lactate conditioning and acidic preconditioning provide a rationale for comparing lactate dose, pH and recipient-cell state in a factorial design[33, 43, 48]. At fixed extracellular lactate, buffering and osmolarity, acute cytokine production and target killing can be measured during exposure, then proliferation and sustained killing after washout. Attenuation of an apparent inhibitory–supportive difference after pH matching would support a pH-dependent contribution under those conditions. If the difference persists, transporter dependence, isotope incorporation and cell state can identify additional mechanisms. A human spatial extension pairs extracellular pH and lactate with recipient phenotype and uptake rather than assigning function from a tumor-average lactate value. A buffered supportive lactate field within an APC–T cell hub or TLS remains a hypothesis.

2.2.4 Lipid composition and oxidative stress

Lipid effects depend on molecular composition and recipient-cell handling. CD36-mediated uptake of oxidized lipids promotes peroxidation and dysfunction in intratumoral $CD8^+$ T cells, with ferroptosis contributing in experimental models[53, 54]. Adipocyte-to-tumor lipid transfer and myeloid-to-dendritic-cell transfer of oxidized lipids have been demonstrated in experimental systems[55, 56], but the sources of lipids encountered by intratumoral T cells require direct localization. Tumor-derived fatty acids carried in extracellular vesicles can support CD36-positive metastasis-associated macrophages in the liver[57]. Breast-cancer brain metastases instead exhibit a dependency on de novo fatty-acid synthesis associated with the local lipid environment[58]. The

contrasting dependencies reflect both the local lipid environment and recipient-cell metabolism. PD-1-dependent phospholipid remodeling[59], tumor-derived fibroblast growth factor 21 (FGF21)[60], and cholesterol deficiency in exhausted T cells[61] identify additional mechanisms, while linoleic acid supplementation can improve $CD8^+$ T cell fitness[62]. Spatial lipid analysis is consequently most informative when registered to cell-specific uptake and oxidative-damage readouts.

Myeloid and stromal responses can differ from those of cytotoxic lymphocytes. Retinoic acid receptor-related orphan receptor gamma (RORγ) links cancer-associated lipid dysmetabolism to myeloid suppression[63], and ACOD1 protects metastasis-promoting neutrophils from ferroptosis[64]. Chemotherapy-conditioned CAF lipid oxidation can instead support T cell cytotoxicity[17]. Bile-acid synthesis introduces an additional constraint on tumor-specific T cells in liver cancer[65], while FLASH radiation altered macrophage lipid metabolism and CAR-T activity in medulloblastoma models[66]. These findings favor testing the relevant lipid species and cell dependency in each context. Broad ferroptosis protection could preserve lymphocytes while also protecting malignant cells, depending on exposure and target distribution[67].

2.2.5 Amino acids and nitrogen-derived products

Tumor-cell SLC43A2-mediated methionine uptake can reduce methionine availability to $CD8^+$ T cells, lowering S-adenosylmethionine and histone H3 lysine 79 dimethylation[68]. This connects substrate acquisition to methyl-donor availability and T cell function, but a transporter-positive tumor boundary does not by itself demonstrate a local depletion zone. A spatial competition model predicts lower extracellular methionine and reduced T cell methyl-donor or histone-methylation readouts near strongly consuming malignant cells after accounting for perfusion and cell density. Tumor-selective SLC43A2 perturbation should change those local measurements before a change in tissue composition is invoked as the explanation. Equivalent extracellular supply despite the functional phenotype would favor additional cell-intrinsic or signaling mechanisms.

Glutamine illustrates how recipient identity and intervention type alter the net response. Competition has been implicated in tumor–myeloid interactions in liver cancer and triple-negative breast cancer (TNBC)[69, 70]. In conventional type 1 dendritic cells (cDC1s), SLC38A2-dependent glutamine acquisition engages folliculin (FLCN) to restrain transcription factor EB (TFEB). Deficiency of SLC38A2 or FLCN impairs cDC1 function and eliminates the benefit of intratumoral glutamine supplementation[71]. By contrast, JHU083, a prodrug of the broad glutamine antagonist 6-diazo-5-oxo-L-norleucine (DON), suppressed cancer-cell glycolytic and oxidative programs while effector T cells adopted greater oxidative metabolism and a persistent activated phenotype[72]. Reduced substrate acquisition in an antigen-presenting cell and pharmacological inhibition of glutamine-utilizing reactions across a tumor expose different dependencies (Table 3B). Their balance also changes with drug distribution, adaptation and the relative importance of priming versus established effector activity.

This distinction yields a timing and localization hypothesis: a treatment that relieves malignant-cell consumption while preserving cDC1 acquisition may support priming, whereas exposure that disables the antigen-presenting recipient could limit it. Matched cDC1–tumor–T cell systems can compare priming-stage with effector-stage intervention while measuring substrate uptake, antigen presentation, T cell expansion and killing. Preserved priming with recipient-directed loss of glutamine acquisition, or benefit unrelated to local supply, would weaken the corresponding competition explanation. In vivo sequencing cannot be inferred from this hypothesis alone: Leone and colleagues observed greater benefit from concurrent than sequential checkpoint treatment in their model[72]. Regional uptake, drug exposure and the limiting immune step must therefore determine the comparison.

Arginine availability adds a related source–sink problem. Increasing intracellular arginine enhanced T cell survival and antitumor activity[73], while myeloid arginase provides a mechanism for extracellular depletion and impaired antigen-specific responses[74]. The spatial prediction is that arginine abundance and recipient function track the balance between supply and local consumption rather than arginase-positive cell density alone. Formate supplementation provides a complementary example of support for one-carbon metabolism and PD-1-blockade efficacy in models[75]. Such support should be evaluated in the responding lymphocyte alongside malignant-cell use of the supplemented substrate.

Tryptophan depletion and accumulation of its products are separable exposures. Kynurenine-associated Siglec-15 or aryl hydrocarbon receptor (AhR) pathways have been linked to suppression, whereas selected microbial tryptophan metabolites support checkpoint responses[76, 77, 78, 79]. A low tryptophan measurement cannot identify the responsible enzyme, and a high kynurenine pool cannot assign production to the nearest cell. Paired substrate–product measurements, source-enzyme

localization and recipient signaling can test whether a suppressive interface reflects nutrient restriction, product signaling or both. Comparisons should also account for vascular delivery and systemic pools, particularly when primary and metastatic lesions occupy different organs.

Ammonia is a nitrogen-derived product rather than an amino acid. Its accumulation promoted T cell exhaustion in colorectal cancer models[80], raising a distinct question about production, assimilation and clearance. Regional total ammonia should be measured with pH because chemical speciation and cellular exposure depend on local conditions. A regional ammonia–dysfunction association should persist after accounting for pH, perfusion and cell composition. Source-selective lowering of ammonia exposure provides a test of this prediction.

2.3 Cell-organized niches

Recurrent arrangements of endothelial, stromal, antigen-presenting and lymphoid cells organize entry, activation, maintenance and exclusion. Spatial imaging establishes these neighborhoods with increasing precision[22, 81, 82, 83, 84]. Their designation as immune niches rests on cellular organization and function; metabolic support is a separate question. This distinction is especially relevant to perivascular APC–T cell hubs and TLS.

2.3.1 Perivascular and APC–T cell niches

Functional vessels can deliver substrates and provide adhesion routes for lymphocytes, whereas poorly perfused or non-adhesive vessels may remain barriers[10, 11]. In experimental tumors, antiangiogenic immune-modulating treatment induced lymphotoxin-dependent conversion of postcapillary venules into high endothelial venule (HEV)-like vessels. These vessels increased lymphocyte entry and supported TCF-1-positive $CD8^+$ populations that differentiated into granzyme B-positive effectors[85]. The result links endothelial state to local T cell organization, but the oxygen tension, nutrient availability and metabolic flux within the associated niches were not directly established.

In human tumors, stem-like $CD8^+$ T cells reside in dense APC niches and can give rise to more differentiated effector populations[86]. Hepatocellular carcinoma treated with PD-1 blockade contained triads of dendritic cells enriched in maturation and regulatory molecules (mregDCs), CXCL13-positive $CD4^+$ helper T cells and progenitor-exhausted $CD8^+$ T cells (TPEX). Responders and nonresponders differed in local clonal expansion and differentiation[87]. Human lung cancers likewise contained stem-immunity hubs associated with response[88]. TCF-1 positivity alone does not identify every population as TPEX: that term requires the chronic-antigen context and corresponding phenotypic or functional evidence. Stem-like, progenitor-exhausted and stem-cell-memory states are related but not interchangeable. cDC1 glutamine sensing and stimulatory cDC1 states support antitumor T cell responses in models[71, 89], yet the glutamine supply of the human APC–T cell niches remains unresolved. Antigen-presenting CAFs may also contribute in selected settings[90].

2.3.2 Tumor interfaces and malignant nests

Spatial studies in colorectal, lung and breast cancer identify immune hubs and mixed or compartmentalized tumor–immune architectures that carry information beyond cell counts[81, 82, 83, 84]. These observations establish tissue organization, not nutrient flux. In non-small-cell lung cancer, GLUT1-positive TAM-rich regions were spatially segregated from $CD8^+$ T cells and associated with resistance to PD-(L)1 blockade. Macrophage-specific SLC2A1 deletion improved T cell distribution and function in experimental tumors[91]. Thus, human spatial association and cell-specific perturbation support a role for macrophage metabolism in immune organization; they do not yet quantify local glucose redistribution between the participating cells.

Interfaces also impose mechanical and energetic demands. Mitochondrial metabolism supports human $CD8^+$ T cell migration through collagen and tumor slices, while phosphoenolpyruvate availability connects glucose metabolism to T cell receptor signaling[92, 93]. Quiescent malignant cells can assemble immune-protective niches[94], and spatial neutrophil programs include context-dependent interactions with fibroblasts and malignant cells[95]. An immune-excluded pattern can therefore arise through failed recruitment, impaired crossing or loss of function after entry. Measuring motility, target contact and killing in sequence helps distinguish these possibilities.

2.3.3 CAF-rich barriers

CAFs remodel tissue architecture and local signaling. In oral squamous cell carcinoma, spatial transcriptomic analyses inferred a lactate-associated epithelial–inflammatory CAF–Treg relationship involving HIF-1α, CXCL12 and transforming growth factor beta (TGF-β)[96]. The study located transcriptional programs and cellular neighbors; the magnitude and direction of lactate transfer were not directly measured. This distinction matters because a proposed metabolic exchange can coexist with chemokine-mediated exclusion without being its established cause.

CAF identity is also adaptable. Macropinocytosis helps maintain CAF subtype programs under nutrient stress in pancreatic cancer[97], whereas glycolytic CAF targeting reduced T cell exclusion and chemoresistance in sarcoma models[23]. Other fibroblast states can support antigen presentation or treatment-associated T cell cytotoxicity[17, 90]. Fibroblast–myeloid niches in tumor-colonized lymph nodes illustrate how stromal organization extends into a distinct anatomical setting[98]. CAF abundance alone is therefore insufficient for selecting an intervention: the relevant state, location, immune partners and metabolic dependency must be specified.

2.3.4 Tertiary lymphoid structures

TLS combine B cell follicles, T cell zones, APCs, stromal organizers and specialized vessels. Mature organization and specific B cell programs have been associated with immunotherapy response and survival[99, 100, 101], with spatial studies resolving helper, B and $CD8^+$ T cell interactions in head-and-neck and nasopharyngeal cancers[102, 103]. B cells can nevertheless inhibit TLS formation in selected settings[104]. Tumor-cell acetyl-CoA acetyltransferase 1 (ACAT1) perturbation altered TLS formation in experimental lung cancer, and clinical specimens linked ACAT1 expression with TLS abundance and treatment outcome[105]. Ovarian cancer studies further demonstrate site- and stroma-dependent TLS activity[106]. These findings support metabolic regulation of niche formation, but do not establish that mature TLS maintain protected oxygen or nutrient concentrations.

Testing metabolic support within TLS requires paired structural, chemical and functional measurements. A proposed workflow would build on tumor-slice culture[107], oxygen sensing in lymph-node slices[108] and pH/lactate monitoring in microfluidic cell culture[109]. Fresh viable slices containing candidate lymphoid aggregates could first undergo calibrated oxygen, pH and lactate measurements under recorded temperature and perfusion conditions. The measured slice can then be fixed for B/T-cell, follicular and vascular mapping, allowing retrospective identification of the TLS core and border using fiducials and tissue landmarks[110]. A neighboring section could be rapidly frozen for targeted MSI[26] and laser-microdissection liquid chromatography–tandem mass spectrometry[111]; glutamine, methionine and arginine assays would require analyte-specific validation and internal standards. These extracts report regional tissue pools, whereas extracellular exposure requires compartment-sensitive sensing or sampling. Comparisons with adjacent viable tumor should account for cell density, tissue composition, vascularity, necrosis and registration error. Paired functional slices could then test whether altering a measured substrate changes local priming or lymphocyte expansion. Measurements obtained after excision describe ex vivo conditions; sampling delay and loss of normal perfusion constrain their relationship to the original in vivo state. A metabolic contribution would be supported if chemistry explained function beyond TLS maturity and composition and if perturbation changed that function without disrupting the structure.

TLS remain inducible. An early intratumoral CD40 agonist study reported mature TLS in complete responders, accompanied by experimental evidence for local immune organization[112]. This is evidence for niche formation and clinical immune activity, not validation of a TLS nutrient-support mechanism. The distinction prevents therapeutic induction of a lymphoid structure from being equated with correction of a measured metabolic field.

2.4 Anatomical context and temporal remodeling

Organ site changes vascular and lymphatic architecture, resident stromal and myeloid populations, nutrient supply and immune regulation. The same malignant clone can therefore encounter different constraints in a primary lesion, draining lymph node or distant organ[9]. Tumor growth, vessel collapse, necrosis and therapy also change these conditions over time. These influences cut across vascular, cellular and physicochemical categories rather than belonging to metabolite production alone.

TNBC illustrates this heterogeneity. Multiplexed imaging identified mixed and compartmentalized tumor–immune architecture[83], while spatial transcriptomics resolved molecular subtypes and tissue archetypes ranging from inflamed or TLS-rich regions to stroma-restricted and immune-desert patterns[113]. These are cellular and transcriptional maps. They provide coordinates for measuring oxygen, adenosine, glutamine or redox conditions, but cannot substitute for those measurements.

Mechanistic work in TNBC linked HEBP2-dependent tumor glutamine use to macrophage ferroptosis and immunotherapy resistance[70]. Separately, serial biopsies after pembrolizumab and radiotherapy identified three response trajectories: persistent poor infiltration in nonresponders, pre-existing immune activation in one responding group, and treatment-emergent interactions between cytotoxic T cells and antigen-presenting myeloid cells in another[114]. The longitudinal study demonstrates cellular remodeling, not direct changes in metabolite

flux. Treatment can also modify substrate uptake or myeloid lipid programs in experimental systems[49, 66]. Interpreting acquired resistance requires distinguishing these observed trajectories from proposed metabolic explanations.

Colorectal liver metastases contain SPP1-positive macrophage–fibroblast networks associated with immunosuppression[115], and hepatic interleukin-10 can promote metastatic immune escape through PD-L1 induction[116]. Brain tumors and metastases display site-specific immune organization[117], while breast-cancer brain metastases can depend on fatty-acid synthesis[58]. A primary-tumor biomarker therefore may not identify the dominant dependency of every metastasis. Matched lesions and comparable time points are needed to separate a conserved tumor program from an organ-imposed constraint.

3. Mapping and interpreting spatial immunometabolic evidence

A study design should begin with the unresolved biological variable. Cell identity and transporter expression locate possible sources and recipients; metabolite measurements describe chemical abundance; physiological sensors measure conditions such as oxygen or pH; isotope incorporation constrains pathway use; and selective perturbations test functional dependence. Spatial transcriptomics and proteomics measure expression and organization, so their pathway scores indicate inferred metabolic capacity. They do not establish reaction rates, substrate availability or exchange direction. MSI annotation[118], integrated metabolite–protein imaging[110] and spatial isotope tracing[119] address complementary parts of this problem. Validation must connect the actual measured quantity to the proposed regional mechanism (Table 4).

3.1 Matching the assay to the material and question

Routine hematoxylin and eosin (H&E), immunohistochemistry (IHC)[120], multiplex immunofluorescence (IF) and RNA in situ hybridization can identify cells, vascular and stromal structures, and enzyme or transporter expression in formalin-fixed paraffin-embedded (FFPE) material. They are useful for discovering and validating spatial associations in clinical archives. Spatial transcriptomics and protein imaging extend molecular coverage and cellular resolution[121, 122, 123], while three-dimensional approaches such as Open-ST and multiplexed tissue atlases help distinguish connected neighborhoods from adjacency in a single section[124, 125]. None of these expression-based methods directly measures soluble-metabolite concentration or exchange. A transcriptional metabolic score should therefore be described as inferred capacity, not as a flux map.

Matrix-assisted laser desorption/ionization (MALDI) and desorption electrospray ionization (DESI) MSI can map metabolites and lipids, usually in frozen material, but nominal mass or accurate mass alone may not resolve isomers or isobaric compounds. Database matching and machine-learning annotation improve prioritization[118], yet confidence in a central analyte requires appropriate standards, fragmentation or an orthogonal targeted assay. Smaller pixels improve localization at the cost of sampled material and often sensitivity or coverage; pixel size is not equivalent to effective biological resolution. Ion suppression and extraction efficiency can produce intensity differences unrelated to concentration. Absolute quantification requires analyte-specific calibration and suitable internal standards. Secondary ion mass spectrometry (SIMS) and vibrational imaging offer different balances of spatial detail and molecular identification, and cannot be treated as universally interchangeable measurements[8].

Integrated spatial metabolite and protein profiling helps assign molecular signals to cellular neighborhoods[110], while imprinting MSI and other spatial metabolomic workflows can provide complementary tissue maps[126, 127]. At a TLS boundary or necrotic margin, however, registration error may be comparable to the distance under study. Same-section analysis can reduce this problem but introduces order-dependent assay effects; adjacent sections may contain different cells. Conventional tissue MSI also does not automatically separate extracellular analytes from intracellular pools. A claim about extracellular exposure requires additional compartment-sensitive evidence, such as calibrated physiological sensing, appropriate sampling or validated biochemical localization.

Genetically encoded sensors can resolve selected exposure dynamics. Laconic uses Förster resonance energy transfer (FRET) to monitor intracellular lactate[128], whereas eLACCO2.1 and R-iLACCO1 report extracellular and intracellular lactate, respectively[129]. Genetically encoded pH-sensitive fluorescent proteins provide another compartment-targeted readout[130]. Sensor localization, affinity, saturation, pH sensitivity, expression and photobleaching require controls, including a nonresponsive construct and calibration under the recording conditions. These tools are best established in experimental preparations; genetic access, delivery and tissue viability limit their use in patient samples. Sensor concentration trajectories become mechanistic evidence when paired with isotope tracing, source- or

recipient-specific perturbation and matched migration, priming or killing assays. A sensor response alone is not a complete flux measurement.

3.2 Isotope tracing and model-based flux inference

Stable-isotope labeling adds information about substrate incorporation and pathway contribution. For example, ^{13}C-SpaceM combines tracing, MSI and microscopy to resolve cellular heterogeneity in de novo fatty-acid synthesis[119]. Label enrichment is nevertheless not a universal measure of absolute flux. Interpretation depends on precursor enrichment, tracer delivery, pool size, labeling duration, recycling and whether the relevant system is near isotopic or metabolic steady state[131]. Label detected in a recipient may derive from a shared circulating substrate rather than transfer from the proposed neighboring source. Alternative routes must therefore be controlled before directionality is assigned.

Table 4. Matching spatial immunometabolic measurements to specimen availability and interpretive limits

Method and question	Material	Actual readout	Principal limitation	Pre-analytical priorities	Biopsy and longitudinal use
H&E and conventional IHC Locate structures and candidate sources/recipients[120]	Usually FFPE	Morphology, cell identity and protein expression; indirect metabolic capacity.	Cannot quantify soluble metabolites or flux; antibody and segmentation dependence.	Fixation time, antigen retrieval, controls and batch effects.	Widely applicable to routine cores and archives; repeated tissue still required.
Multiplex IHC/IF and spatial proteomics Resolve cellular neighborhoods[122, 154]	FFPE or frozen; protocol dependent	Protein-defined cell states, distances and interfaces.	Finite panels and segmentation/registration error; not direct nutrient measurement.	Fixation, staining cycles, antibody validation and tissue loss.	Useful in clinical blocks; serial samples are destructive and may differ in site.
RNA in situ hybridization and spatial transcriptomics Localize expression programs[121, 123, 124]	Fresh/frozen or FFPE; platform dependent	RNA abundance, cell-type inference and tissue organization.	RNA does not establish enzyme activity, metabolite concentration or transfer.	RNA integrity, fixation compatibility, capture efficiency and section order.	Routine-biopsy compatibility varies; archival comparisons need batch control.
MALDI/DESI MSI Map identified metabolites and lipids[26, 118]	Usually fresh frozen; analyte dependent	Ion distributions and relative abundance; quantitative assays require calibration.	Isomers, ion suppression and resolution–coverage tradeoff; intra-/extracellular pools may mix.	Ischemia, rapid quenching, storage, washing, matrix/solvent application and standards.	Core use depends on material and analyte sensitivity; repeat sampling required.
SIMS and vibrational imaging Probe small-scale chemistry[8]	Fixed/frozen or live preparations, method dependent	Secondary-ion or vibrational signals; targeted tracer information where applicable.	Molecular fragmentation or spectral ambiguity; sensitivity and coverage vary.	Preparation chemistry, calibration, laser/ion conditions and preservation.	Specialist research workflows; not universally deployable in serial patient biopsies.
Integrated metabolite–protein imaging Assign signals to cell neighborhoods[110]	Platform-specific tissue preparations	Registered metabolic signals and protein-defined cell identities.	Alignment and processing order can change signal; proximity is not exchange.	Section matching, assay sequence, fiducials and registration error.	Material-intensive; valuable in selected patient samples.
Calibrated oxygen/pH sensors[108, 109]	Fresh viable slices or in vivo research	Oxygen or pH at the probe/recording scale; dynamic exposure when repeatedly sampled.	Local calibration, compartment and ex vivo perfusion differ from intact tissue.	Temperature, reoxygenation, slice thickness, perfusion and recording delay.	Research use in accessible preparations; repeat clinical access is constrained.
Encoded lactate sensors: Laconic/eLACCO[128, 129]	Genetically accessible viable cells, slices or experimental animals	Intracellular FRET signal with Laconic; extracellular eLACCO or intracellular R-iLACCO concentration dynamics.	Affinity/saturation, pH sensitivity, localization and expression; concentration dynamics alone are not full flux.	In situ calibration, nonresponsive controls, photobleaching and registration to recipient identity.	Established mainly in models; genetic delivery and viable tissue limit patient-biopsy deployment.
Encoded pH-sensitive fluorescent proteins[130]	Genetically accessible viable preparations	pH-dependent fluorescence in the targeted compartment.	Intracellular or vesicular localization cannot automatically describe extracellular pH; construct-specific calibration.	Localization control, dynamic range, buffering, temperature and photobleaching.	Experimental validation tool; routine fixed tissue cannot supply live exposure history.
Stable-isotope tracing and ^{13}C-SpaceM Constrain substrate use[119]	Labeled experimental systems; selected clinical sampling	Isotopologue enrichment and pathway contribution.	Absolute flux requires kinetic/pool assumptions; common precursors confound source attribution.	Tracer enrichment, administration and sampling times, quenching and recycling.	Useful in selected surgical/window studies; not routine repeated cell-resolved tracing.
spFBA and patient-specific flux models Test feasible metabolic programs[15, 132]	Depends on transcriptomic and tracer inputs	Model-conditioned flux estimates or feasible exchange patterns.	Network, steady-state, objective and exchange assumptions; non-unique solutions.	Input normalization, boundary definition, data quality and sensitivity analysis.	May reuse existing data; clinical predictions require independent validation.
PET and metabolic MRI Follow lesion-scale change[8]	In vivo	Tracer uptake or modality-specific metabolic/physiological signals.	Limited cellular specificity and spatial resolution; no direct cell-to-cell direction.	Tracer protocol, uptake interval, motion and cross-scan calibration.	Repeat assessment can be feasible; some metabolic MRI approaches remain investigational.
Digital pathology and virtual proteomics Extend assessment across archives[101, 155]	Routine H&E and matched training data	Structural features and predicted protein/TLS states.	Predictions are not direct metabolite or flux measurements; domain shift.	Staining/scanner variation; patient/center-level data separation and calibration.	Scalable on available blocks; repeat observation still needs tissue or validated imaging.

Direct describes the analyte or physiological quantity actually measured, not automatic proof of causation or absolute concentration. A research platform compatible with a small specimen is not necessarily validated for routine clinical biopsies. H&E, hematoxylin and eosin; IHC, immunohistochemistry; IF, immunofluorescence; FFPE, formalin-fixed paraffin-embedded; MALDI, matrix-assisted laser desorption/ionization; DESI, desorption electrospray ionization; MSI, mass spectrometry imaging; SIMS, secondary ion mass spectrometry; spFBA, spatial flux balance analysis; PET, positron emission tomography; MRI, magnetic resonance imaging; TLS, tertiary lymphoid structure.

Human spatial tracing is constrained by tracer administration, clinical scheduling, variable perfusion, limited tissue volume and the need to preserve rapidly changing metabolites during sampling. Surgical or window studies can answer selected questions, but repeated cell-resolved in vivo tracing is not a routine clinical assay. Patient-specific metabolic models can integrate available measurements[132], yet model output remains conditional on the measurements and assumptions supplied. spFBA additionally depends on a reconstructed reaction network, steady-state mass balance, exchange bounds, transcript-to-reaction constraints and an objective or optimization rule[15]. Multiple feasible solutions and uncertain tissue boundaries limit the certainty of individual reaction directions. Sensitivity analysis and independent isotope, biochemical or perturbation evidence are necessary before a predicted exchange is treated as an endogenous mechanism.

3.3 Evaluating causality and pre-analytical uncertainty

Evidence for source-to-recipient transfer should be assessed in stages. First, establish the identity of the chemical signal and the relevant spatial and temporal scale. Next, determine whether the candidate source and recipient are positioned within a plausible interaction range. Tracer entry into the recipient should then be tested against shared-substrate exposure and alternative sources. Finally, source- or recipient-specific perturbation should alter transfer and the proposed immune outcome. Spatial CRISPR can identify regulators of local cell organization[133], but that result alone does not establish metabolite exchange. High transporter expression need not mean high uptake, high abundance need not mean high production, and two-dimensional proximity need not indicate cell contact. A study can provide strong functional evidence in a model while leaving the spatial mechanism in patients unresolved.

Pre-analytical effects differ by platform. Warm and cold ischemia can alter energy and redox metabolites before freezing; washing and solvent-based matrix application can extract or redistribute analytes during MSI. Fixation duration, antigen retrieval and antibody performance affect IHC/IF, whereas RNA integrity and fixation compatibility affect RNA-based assays. Fresh-tissue sensors are sensitive to calibration, temperature, oxygen exposure, slice thickness and perfusion. Tracer studies require documentation of the administered substrate, enrichment, infusion-to-sampling interval and quenching conditions. These variables, together with registration error and missing tissue, should be reported alongside the biological result[8, 118, 119]. Integrated gastric and pancreatic cancer studies illustrate the value of combining cell states with molecular maps[134, 135], but reproducibility depends on distinguishing measured chemistry, inferred capacity and ex vivo changes.

4. Spatial metabolic control of immune-cell fate

Metabolic conditions can affect distinct steps of the antitumor immune response, including tissue entry, antigen presentation, migration, target-cell contact, differentiation and persistence[3, 4, 5, 85, 86, 87, 92, 93]. A single metabolic alteration may influence several of these processes, so functional failure is better resolved at the level of the affected step than inferred from lymphocyte abundance alone. Current position and prior exposure can also have different consequences for immune-cell behavior, motivating separate consideration of immediate dysfunction and recoverability (Figure 2).

4.1 Entry and local renewal

Functional perfusion and endothelial adhesion determine whether lymphocytes can reach tissue, while mitochondrial metabolism supports movement after extravasation[85, 92]. Successful entry does not guarantee productive target contact. APC-rich niches can maintain progenitor populations and support effector differentiation[86, 87, 88], complementing activation in draining lymph nodes[136]. A renewing pool may nevertheless remain separated from malignant nests by a poorly traversable interface. The relevant functional measurements are therefore entry, local expansion and effector movement, with direct metabolic measurements needed to determine the contribution of oxygen or nutrient support.

4.2 Interface traversal and effector function

Movement through matrix, immunological-synapse formation and repeated killing impose different metabolic demands. Mitochondrial inhibition can impair migration in human T cells even when a conventional suspension assay does not reproduce the tissue barrier[92], whereas phosphoenolpyruvate availability regulates T cell receptor signaling[93]. The functional interpretation of a metabolic interface therefore depends on where failure occurs. In the GLUT1-positive TAM example, imaging and macrophage-specific intervention support altered T cell distribution and activity[91]. In the SLC43A2 system, biochemical and genetic evidence links tumor methionine consumption to T cell methylation and function[68]. These findings illustrate mechanistically distinct causes of impaired T cell function at an interface. Paired uptake, migration,

target-contact and killing measurements can distinguish resource restriction from failed access or signaling and establish whether an intervention restores the limiting step.

4.3 Organelle transfer, vesicle cargo and extracellular signaling

Intercellular metabolic influence extends beyond soluble substrates, but the route and direction of benefit differ. Clinical specimens have revealed mitochondrial DNA variants shared by cancer cells and TILs. Experimental work showed that tumor-derived mitochondria carrying dysfunctional mitochondrial genomes can transfer to T cells, evade mitophagy and impair their metabolism and immune function[19]. The effect should therefore be attributed to the tested donor organelles and recipient context rather than to every form of mitochondrial transfer. Human validation requires source-associated variants, single-cell localization and exclusion of doublets, attached fragments and contamination. A contact-associated spatial model predicts enrichment of donor-marked organelles in exposed recipients, with function related to transferred burden or organelle quality. Transfer blockade and matched functional testing are needed to separate organelle-mediated injury from a shared stressful environment; complete endogenous trajectories and prevalence across human cancers remain unresolved.

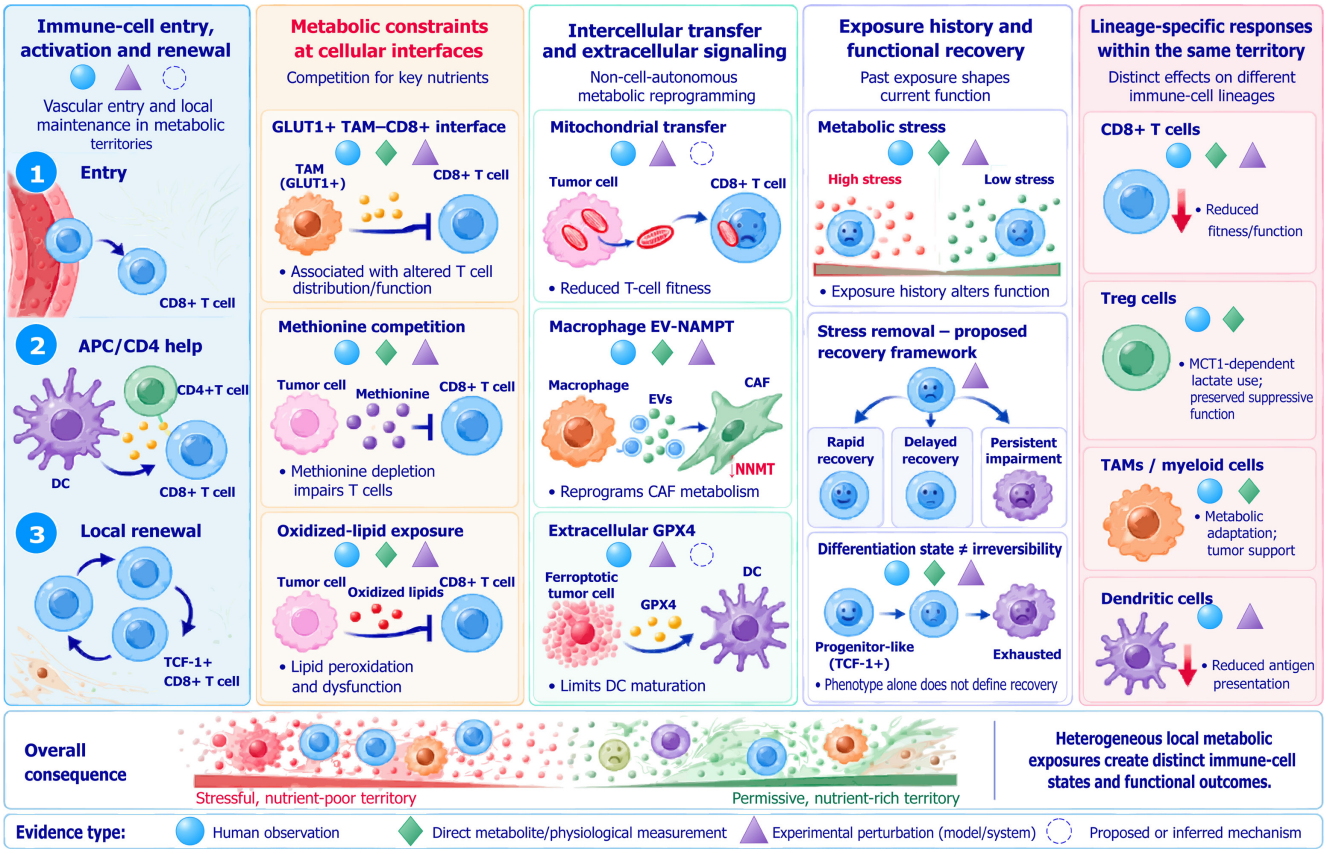

Figure 2. Spatial metabolic territories shape immune-cell fate and functional outcomes. Representative consequences are organized into five dimensions: immune-cell entry, activation and renewal; metabolic constraints at cellular interfaces; intercellular transfer and extracellular signaling; exposure history and functional recovery; and lineage-specific responses. The first panel links vascular entry with APC/CD4-help-associated CD8-positive T-cell activation and local renewal; TCF-1 expression alone does not establish renewal capacity. The second panel distinguishes GLUT1-positive TAM-associated changes in T-cell distribution and function from methionine competition and oxidized-lipid exposure. Human TAM–T-cell spatial segregation and experimental macrophage-specific perturbation support a functional relationship, but do not by themselves establish direct local glucose competition. The third panel depicts tumor-to-T-cell mitochondrial transfer, macrophage NAMPT-containing extracellular vesicles that suppress CAF NNMT, and extracellular GPX4 binding to ZP3 on the dendritic-cell surface to limit maturation. The GPX4 mechanism does not require vesicle uptake. In the fourth panel, stress-removal outcomes form a proposed recovery framework, while differentiation state and recoverability are treated as separate dimensions. Rapid recovery, delayed recovery and persistent impairment are outcomes under defined recovery conditions rather than categories already validated together in human tissue. The fifth panel illustrates selected lineage-specific responses under suppressive metabolic conditions, including MCT1-dependent lactate use by Tregs and context-dependent myeloid adaptation. Blue circles indicate human observations, which may be spatial or non-spatial; green diamonds indicate direct metabolic or physiological measurements; purple triangles indicate experimental perturbation; and dashed circles indicate proposed or inferred mechanisms. Symbols identify evidence types represented in the relevant literature rather than support for every statement within a box, a unified evidence score, or proof that all measurements were obtained in the same study or patient region. APC, antigen-presenting cell; CAF, cancer-associated fibroblast; DC, dendritic cell; EV, extracellular vesicle; GPX4, glutathione peroxidase 4; GLUT1, glucose transporter 1; MCT1, monocarboxylate transporter 1; NAMPT, nicotinamide phosphoribosyltransferase; NNMT, nicotinamide N-methyltransferase; TAM, tumor-associated macrophage; TCF-1, T cell factor 1; Treg, regulatory T cell; ZP3, zona pellucida glycoprotein 3.

Macrophage-derived extracellular vesicles containing nicotinamide phosphoribosyltransferase (NAMPT) engage a distinct regulatory circuit in gastric cancer. In CAFs, the Notch transcription factor RBP-J activates nicotinamide N-methyltransferase (NNMT); vesicle-associated NAMPT suppresses NNMT through the sirtuin 1 (SIRT1)/Notch intracellular domain (NICD) axis. Autologous vesicle administration restored $CD8^+$ T cell cytotoxicity and anti-PD-1 activity in experimental systems, while patient transcriptomic and serial plasma observations supported pathway relevance[20]. Exogenous delivery establishes therapeutic potential within those systems but does not quantify endogenous cargo delivery to individual human CAFs. Spatial analysis should relate macrophage-derived vesicle uptake to CAF NNMT, nicotinamide/1-methylnicotinamide balance and nearby $CD8^+$ function. Source or cargo depletion, dose-matched free NAMPT and uptake controls would distinguish vesicle-associated activity from soluble enzyme effects. The effective range will depend on transport and recipient access rather than macrophage–CAF proximity alone.

Extracellular glutathione peroxidase 4 (GPX4) released during cancer-cell ferroptosis instead binds zona pellucida glycoprotein 3 (ZP3) on dendritic cells, inhibits their glycolysis and impairs maturation and T cell priming. Blockade restored immune activity in preclinical models; circulating GPX4 and dendritic-cell ZP3 were associated with clinical treatment resistance[21]. This is extracellular ligand–receptor signaling rather than a requirement for vesicle uptake. A local-release model predicts that GPX4 exposure and ZP3 engagement precede impaired maturation in DCs near ferroptotic tissue, with the pattern modified by protein transport and clearance. Paired receptor-engagement and functional assays, including ZP3-dependent blockade, can test that prediction. Interventions should distinguish this extracellular interaction from intracellular GPX4-dependent protection against lipid peroxidation. Across these mechanisms, spatial proximity nominates a route; source attribution, physiologically relevant exposure and recipient-specific rescue establish its contribution.

4.4 Exposure history and functional recovery

Current position may not explain current function because an earlier metabolic stress can affect subsequent differentiation. Methionine restriction during early T cell activation produced impairment that was not fully corrected by later restoration of methionine[137]. Mitochondrial dysfunction and LARP4-dependent hypertranslation can also reinforce persistent T cell abnormalities[31, 32]. Meanwhile, checkpoint responses may involve new or expanded tumor-reactive clonotypes rather than recovery of every resident cell[138]. A functional T cell found after treatment therefore does not necessarily represent reversal of damage in the population sampled before treatment.

Differentiation state and functional recoverability describe different dimensions of a T cell response. Phenotype can identify progenitor-exhausted or terminally differentiated populations, while recovery assays ask whether a specified function returns after a defined stress is removed. Exposure history includes concentration, duration, repeated episodes and their order. Live sensors and controlled exposure protocols can record these trajectories; serial biopsies sample population-level change, whereas an endpoint transcriptional or chromatin signature provides an exposure proxy rather than a direct reconstruction. Fresh tumor slices can preserve neighborhoods for initial chemical and functional measurements[107], followed by testing of matched TILs under recorded nutrient, pH, oxygen, cytokine and antigen-stimulation conditions. A pilot can predefine measurements immediately after stress removal and at 24 and 72 hours, adjusting the intervals to the cell system. These are example intervals, not a universal recovery standard. Unexposed, continuously exposed and recovery groups should be compared at matched viability and viable effector number, using immediate signaling or cytokines alongside proliferation and serial killing. Mitochondrial function, oxidative damage and chromatin state can explain delayed or incomplete recovery. Dissociation and oxygen delivery introduce additional effects[107, 139]; shared T cell receptor clonotypes support population comparison without proving recovery of the same individual cells.

IL-10-mediated metabolic reprogramming enhanced antitumor activity in terminally exhausted $CD8^+$ T cells in experimental models[140], demonstrating why differentiation alone cannot establish irreversibility. A stress-associated transcriptional state can identify populations for functional testing[141], but the result should be reported as recovery or persistent impairment under the conditions examined. Separately recording phenotype and recovery makes it possible to ask whether tissue conditioning restores resident-cell activity or whether additional functional cells are needed.

4.5 Lineage-specific responses

Cytotoxic and regulatory cells can respond differently to the same environment. Tregs use MCT1-dependent lactate metabolism and forkhead box P3 (FOXP3)-associated programs to maintain activity

under conditions that impair effector T cells[45, 46, 47]. Their stability also depends on antioxidant regulation, including TMED4-mediated ER and reactive oxygen species homeostasis in models[142]. cDC1 glutamine sensing supports priming[71], while extracellular GPX4 compromises dendritic-cell activation[21]. Neutrophil responses include ACOD1-dependent ferroptosis resistance, hypoxia-driven EGR1 activity and lactylation-associated suppressive programs[28, 29, 64]. Spatial profiling also identifies antigen-presenting and other context-dependent neutrophil states[95], and myeloid-derived suppressor cells couple immunoregulatory and pro-angiogenic programs[143]. Their effects cannot be inferred from total myeloid abundance.

Natural killer (NK) cells deserve separate consideration. Lactic acid can reduce their interferon-γ production and survival[43]. In obesity, lipid accumulation driven by peroxisome proliferator-activated receptors impaired NK-cell metabolism and delivery of cytotoxic machinery to the tumor-cell synapse; metabolic intervention restored function in experimental systems[144]. These are lineage-specific functional results, not complete spatial maps of NK-cell exposure in human tumors. Chimeric antigen receptor-engineered NK cell (CAR-NK) screens nominate additional targets for improving antitumor activity[145], but the clinical maturity of the cell platform does not validate a particular metabolic edit. Innate lymphoid cells (ILCs) are likewise heterogeneous. Type 2 ILCs (ILC2s) enhanced tissue-specific immunity and PD-1-blockade activity in pancreatic cancer models, with corresponding populations detected in human tumors[146]. The oxygen and nutrient conditions supporting those cells remain unresolved and should not be extrapolated from NK or $CD8^+$ T cells.

B cells and helper T cells contribute through organized APC–T cell hubs and TLS, where maturation and cellular interactions are more informative than lineage counts alone[87, 102, 103]. Because B-cell effects can be supportive or suppressive[104], a metabolically favorable niche for one population need not support all antitumor functions. Comparing uptake, redox state, migration and recovery across neighboring lineages would reveal whether a region preserves cytotoxic immunity or preferentially sustains regulatory and stromal functions. Across these lineages, direct human spatial-metabolic measurements remain uneven, so breadth of coverage should not be interpreted as equivalent evidentiary maturity.

5 Regional treatment resistance and sampling limitations

Regional treatment resistance can arise when immune activity is restored in some parts of a lesion but remains constrained in others. Incomplete contact between functional immune cells and viable malignant regions may therefore persist even when average immune infiltration increases. Spatial association and model perturbation studies support components of this possibility[14, 26, 34, 91], but incomplete spatial coverage has not been established as a general causal predictor of clinical resistance. Its contribution should be evaluated alongside antigen loss, impaired presentation, altered interferon signaling and other established mechanisms of primary or acquired resistance[147, 148].

5.1 Checkpoint blockade and heterogeneous residual disease

Checkpoint inhibition may expand or reinvigorate tumor-reactive cells without removing the conditions that restrict their access or function. The relevant question is whether immune activation reaches viable tumor regions and produces sustained target engagement, rather than whether total $CD8^+$ T cell density rises. Macrophage-associated segregation and peri-necrotic metabolic stress identify candidate barriers[26, 91], but an association between these features and resistance does not prove that they are the dominant cause in an individual patient. Functional and spatial changes should be related to the location of residual disease.

The TNBC pembrolizumab–radiotherapy study provides a longitudinal example: responding and nonresponding tumors followed different cellular trajectories despite receiving the same regimen[114]. Paired baseline, early-treatment and residual or progressing samples can distinguish persistence of an original barrier from changes in cellular composition. Apparent enrichment of a suppressive population may reflect preferential survival or shrinkage of another compartment rather than a newly induced program. Clonal replacement after PD-1 blockade further complicates attribution[138]. These possibilities require comparable lesion sites and explicit accounting for viable tumor, necrosis and treatment timing before cellular remodeling is called metabolic adaptation.

5.2 Adoptive cell therapy

Infused lymphocytes encounter conditions unlike those used during manufacturing. Tumor glycolysis, endothelial metabolism and radiation-associated myeloid lipid programs have each affected

access or activity in experimental cellular-therapy studies[14, 66, 149]. Expansion in blood or cytotoxicity in nutrient-replete culture therefore does not establish effective tumor coverage. Regional accumulation, migration into malignant nests, repeated target contact and persistence should accompany systemic and bulk-tumor endpoints. These measurements distinguish a limitation of the cell product from a receiving-tissue barrier and provide a rationale for testing metabolic engineering under sequential, rather than isolated, tissue stresses.

5.3 Cytotoxic and vascular therapies

Radiotherapy, chemotherapy and vascular treatment alter cell death, perfusion and tissue repair. An early inflammatory response may coexist with later debris accumulation or hypoxic viable tissue. Vascular normalization can improve access, whereas excessive pruning may worsen oxygen limitation[10, 11]. Preclinical STING-based vascular remodeling and metformin-associated vascular changes provide examples of altered immune access[150, 151], while radiation modality changed macrophage lipid programs in medulloblastoma[66]. These findings should not be generalized to a common clinical treatment sequence. The useful comparison is between early and delayed perfusion, antigen-presenting competence, immune-cell movement and residual viable tumor.

5.4 Clinically feasible spatial sampling

A core biopsy samples a limited region. Lung and melanoma imaging studies show spatial immune organization associated with outcome[82, 152, 153], while ovarian cancer TLS activity varies by anatomical site[106]. A single positive core may overrepresent a small immune-active hub, and a negative core may miss one. Multiple blocks or regions can help when available, but repeated multiregion biopsy is not routinely feasible for many patients. A practical approach uses clinically indicated biopsies and surgical material, with image guidance to select representative viable tissue when safe and appropriate. The sampled site, minimum evaluable area, necrotic fraction and missing regions must be reported.

Non-invasive imaging and routine pathology can partially extend coverage. Positron emission tomography (PET) or magnetic resonance imaging (MRI) can follow lesion-scale changes[8], although fluorodeoxyglucose uptake reflects several cell populations and does not establish cell-to-cell transfer. H&E, multiplex IHC/IF and digital pathology can assess tissue architecture across available blocks[121, 122]. High-resolution spatial proteomics can refine cell identity[154], and virtual protein maps can generate predictions from histology[155], but neither is a direct soluble-metabolite assay. These approaches are most useful when validated against the molecular feature they approximate. One accessible lesion cannot represent every metastasis, and missing tissue should be treated explicitly rather than excluded without accounting.

5.5 Metabolic heterogeneity and therapeutic evolution

Treatment can remodel a metabolic territory by changing malignant clones, reversible cellular states, stromal partners and tissue supply. Within-clone plasticity and selection of pre-existing subclones may produce similar expression patterns but imply different interventions[9]. Using lineage barcodes, Oren and colleagues found that cycling and noncycling drug-tolerant persisters arose from distinct lineages and differed in metabolic programs. Fatty-acid oxidation and antioxidant programs were associated with proliferation under continued targeted therapy, and perturbing these programs altered the cycling persister fraction[156]. LDH inhibition could, for example, enrich cells able to sustain greater oxidative metabolism. This is a selection hypothesis rather than an established consequence of the LDH regimen that redistributed glucose uptake in tumor models[49]. Pre-existing oxidative cells may expand, surviving cells may switch state, or improved oxygen delivery may permit a different program. Each would produce a different relationship between clonal identity, position and substrate use.

Linking these lineage–state relationships to a metabolic territory requires longitudinal regional isotope measurements paired with lineage barcodes or somatic variants in models and selected patient material. Expansion of the same pretreatment oxidative lineage would support selection; a reversible metabolic shift within a stable lineage would support plasticity. Repeated assessment of perfusion, immune composition and viable tumor is needed because altered supply or loss of neighboring cells can mimic intrinsic adaptation. Withdrawal and rechallenge experiments can test reversibility, while functional inhibition of the emergent dependency determines whether it contributes to resistance. Antigen loss and other established resistance mechanisms remain competing explanations[147, 148].

Immune cells can also retain effects of earlier exposure after the environment changes. Early methionine availability influenced later exhaustion in experimental T cells[137]. More generally, tumor-specific T cell dysfunction is associated with chromatin

states that differ in reprogrammability[157]. The latter evidence establishes a basis for persistent immune states but does not attribute every epigenetic alteration to metabolism. A metabolically induced, mitotically persistent change would require matched exposure and washout, tracking across cell division and functional testing under a common environment. Selective survival, persistent antigen and replacement by newly recruited clonotypes must be excluded before improved tissue function is assigned to recovery of previously injured cells[138]. These temporal distinctions connect treatment evolution to the recovery assays described above.

6. Therapeutic evidence and spatial translation

Clinical translation requires separating pathway activity from validation of a biomarker that can guide treatment. A metabolic intervention may show pharmacological activity without establishing that a proposed spatial feature predicts benefit, and shared dependencies in malignant and immune cells can make the therapeutic index context dependent[5]. Representative IDO1 and CD73 studies illustrate the distinction between early target engagement, randomized efficacy and subsequent phase III development[158, 159, 160, 161, 162]. ECHO-301, the first-in-human oleclumab study, COAST and COLUMBIA-1 provide reported outcomes, whereas PACIFIC-9 illustrates phase III evaluation without efficacy results in the cited design report. These clinical examples are summarized in Table 5; Table 6 separately presents experimental regional intervention strategies and proposed pharmacodynamic readouts.

6.1 Clinical evidence from IDO1 and CD73 inhibition

In ECHO-301/KEYNOTE-252 (NCT02752074), 706 patients with unresectable or metastatic melanoma were randomized to the indoleamine 2,3-dioxygenase 1 (IDO1) inhibitor epacadostat 100 mg twice daily or placebo, each combined with pembrolizumab. Median progression-free survival (PFS) was 4.7 versus 4.9 months (hazard ratio [HR], 1.00; 95% confidence interval [CI], 0.83–1.21), and overall survival (OS) was not improved (HR, 1.13; 95% CI, 0.86–1.49)[158]. The negative phase III result applies to the regimen and population tested. It does not show that absent spatial patient selection caused failure. Pharmacodynamic adequacy, alternative tryptophan-catabolic pathways, drug exposure and disease heterogeneity remain distinct explanations that cannot be resolved retrospectively from unmeasured spatial variables.

Table 5. Representative clinical evidence for metabolic-pathway interventions

Study and target	Population and regimen	Design and report status	Key reported outcome	Biomarker strategy	Spatial interpretation
ECHO-301/KEYNOTE-252 IDO1; epacadostat NCT02752074[158]	Unresectable/metastatic melanoma. Epacadostat 100 mg twice daily + pembrolizumab versus placebo + pembrolizumab.	Randomized phase III; n=706. Published 2019; stopped for lack of benefit. Registry: completed.	Median PFS 4.7 versus 4.9 months; HR 1.00 (95% CI 0.83–1.21). OS HR 1.13 (0.86–1.49). No efficacy improvement.	PD-L1/BRAF stratification; no validated spatial kynurenine-based selection.	Failure does not identify absent spatial selection as its cause.
Oleclumab first-in-human CD73 NCT02503774[159]	Advanced solid tumors. Oleclumab alone or with durvalumab; CRC, PDAC and EGFR-mutant NSCLC expansion cohorts.	Phase I; n=192 overall; 42 per expansion cohort. Published 2023. Registry: completed.	Expansion-cohort ORR 2.4%, 4.8% and 9.5%, respectively. Target engagement and manageable safety; no randomized survival comparison.	CD73 pharmacodynamics and exploratory tissue biomarkers.	Feasibility of pathway inhibition, not validation of local adenosine selection.
COAST CD73; oleclumab NCT03822351[160]	Unresectable stage III NSCLC without progression after concurrent chemoradiotherapy. Durvalumab + oleclumab versus durvalumab; separate monalizumab arm.	Randomized phase II; n=189 across all arms. Final analysis published 2025; data cutoff 18 July 2023. Registry: completed.	ORR 35.0% versus 23.9%, difference not significant. PFS HR 0.59 (0.37–0.93); OS HR 0.69 (0.40–1.20).	Exploratory biomarker analyses; no prospectively validated spatial adenosine classifier.	Phase II PFS signal; no established OS benefit or spatial predictive biomarker.
PACIFIC-9 CD73; oleclumab NCT05221840[161]	Unresectable stage III NSCLC without progression after concurrent chemoradiotherapy. Durvalumab + oleclumab or monalizumab versus durvalumab + placebo.	Double-blind randomized phase III. Protocol published 2024. Registry: active, not recruiting; no results posted at check.	Design report only. Primary endpoint: blinded independent central review PFS. No phase III efficacy estimate in the cited report.	Protocol includes tissue-based exploratory analyses; no validated spatial adenosine selection rule.	Phase III development following COAST; trial design is distinct from demonstrated efficacy.
COLUMBIA-1 CD73; oleclumab NCT04068610[162]	Previously untreated MSS metastatic CRC. FOLFOX + bevacizumab + durvalumab + oleclumab versus FOLFOX + bevacizumab.	Phase Ib safety cohort n=7; randomized phase II n=52. Published 2024. Registry: active, not recruiting.	Randomized ORR 61.5% versus 46.2%, not significant. Results did not support further development of this combination in this population.	Exploratory CD73 and related biomarkers.	Does not establish failure of the entire CD73 target class or test spatial selection.

Reported efficacy and registry status are distinct. Registry information was checked on 14 September 2026: NCT02752074 last updated 24 August 2025; NCT02503774, 11 July 2023; NCT03822351, 8 October 2024; NCT04068610, 11 August 2026. NCT05221840 was checked on 14 September 2026 (last updated 18 June 2026; no results posted). The studies were selected narratively to compare trial stages and tumor contexts. Published results should not be interpreted as a later unreported analysis. HR, hazard ratio; CI, confidence interval; PFS, progression-free survival; OS, overall survival; ORR, objective response rate; CRC, colorectal cancer; PDAC, pancreatic ductal adenocarcinoma; NSCLC, non-small-cell lung cancer; MSS, microsatellite stable; IDO1, indoleamine 2,3-dioxygenase 1.

Table 6. Experimental interventions and requirements for regional translation

Target or barrier	Evidence and intended recipient	Safety and selectivity questions	Regional delivery and target engagement	Lead-in or functional test	Adaptation and trial interpretation
Vascular/stromal access[13, 14, 23, 150]	Endothelial STING/PHGDH or glycolytic CAF modulation; preclinical evidence.	Preserve functional vessels, supportive fibroblast states and APC-rich niches; depletion alone is insufficient.	Confirm tissue exposure, perfusion, viable hypoxic fraction and stromal state; quantify access to malignant regions.	Compare conditioning before CAR-T with concurrent treatment where justified by early perfusion changes.	Distinguish vessel pruning, altered tumor composition and persistent structural barriers from restored immune access.
Extracellular acidosis[34]	Tumor-cell SLC4A4 inhibition in pancreatic cancer models.	Tumor versus normal-tissue transporter effects; recipient intracellular pH and viability.	Calibrated extracellular pH plus tumor target inhibition; test local coverage and systemic exposure.	A pH-correcting lead-in is justified only if early pH change precedes the proposed immune benefit.	Persistent dysfunction after pH correction may reflect injury history or a second barrier.
LDH inhibition[49]	Tumor-model glucose redistribution with immune functional benefit.	Shared glycolytic requirements in malignant and activated immune cells; cell-specific therapeutic window.	Regional drug and LDH activity, extracellular lactate/pH and tumor-versus-immune glucose uptake.	Link early pathway inhibition to later migration/killing; compare concurrent and lead-in strategies.	Track oxidative states and clonal identity; an oxidative shift is a candidate adaptation until functionally tested.
MCT11 blockade[44]	Recipient-directed lactate uptake in exhausted T cells; genetic/antibody model evidence.	Cell-state selectivity, other-tissue expression and reagent specificity; avoid extrapolating genetic selectivity to any drug.	Target-cell uptake and function with target-deficient or other specificity controls; document tissue penetration.	Measure acute cytokines and sustained killing separately; determine whether a lead-in adds an early tissue effect.	Check alternative transport/recipient states and continuing exposure. Total tissue lactate alone is an inadequate engagement assay.
Tumor SLC43A2[68]	Tumor methionine acquisition and T cell methyl-donor metabolism; biochemical/genetic evidence.	Preserve T cell uptake and normal-tissue substrate needs; systemic deprivation has different consequences.	Tumor-selective delivery/perturbation, local methionine, recipient S-adenosylmethionine and histone methylation.	Require a change in recipient metabolism before claiming reversal of substrate competition.	Assess alternative transport, remaining sources/sinks and persistent chromatin or functional abnormalities.
Lithium-associated lactate routing[167, 168]	Preclinical restoration of tumor-reactive $CD8^+$ metabolism.	Concentration-related toxicity; renal, fluid/electrolyte, neurological and interacting-drug considerations.	Serum and tumor exposure, recipient lactate handling/mitochondrial readouts and matched viable-cell function.	No established oncology lead-in. Determine tolerability and tissue pharmacodynamics before sequencing claims.	Existing clinical use in another indication does not validate a tumor-immunity dose or regional mechanism.
Glutamine strategies[71, 72]	cDC1 support versus broad antagonism; recipient- and regimen-dependent experimental effects.	Preserve priming and other glutamine-dependent immune functions while suppressing malignant cells.	Drug or substrate distribution, cDC1/tumor/T cell uptake and paired priming/effector assays.	Compare priming-stage and effector-stage exposure. Concurrent treatment was favored in the cited JHU083 checkpoint model.	Measure metabolic adaptation and recipient replacement rather than interpreting all interventions as nutrient withdrawal.
Transfer or extracellular signaling[19, 20, 21]	Tumor mitochondria, macrophage NAMPT vesicles or extracellular GPX4–ZP3; distinct model mechanisms.	Donor/cargo quality, free versus vesicle-associated NAMPT, extracellular versus intracellular GPX4 effects.	Source attribution, recipient uptake for cargo, or surface engagement for GPX4; pair with functional rescue.	Match intervention to transfer, cargo action or receptor signaling instead of a shared uptake endpoint.	Confirm endogenous exposure and range; exogenous vesicle dosing and circulating markers do not define local mechanism.
Therapeutic lymphocyte fitness[173, 174, 176, 177, 178]	PKM2/P4HA1, NAD/IDH2 or ketone-related experimental strategies.	Modification-specific viability, differentiation and function under sequential tissue stresses.	Regional persistence, target contact, mitochondrial fitness and sustained killing; cell-product expansion alone is insufficient.	Test hypoxia, acidity, nutrient restriction and matrix traversal in relevant order, followed by recovery.	Clinical maturity of a cell platform does not establish benefit from a particular metabolic modification.

These are experimental strategies. Local delivery requires measured coverage, retention and systemic leakage. Lead-in duration follows pharmacokinetics and a prespecified tissue effect. Delivery, target engagement, regional chemistry, recipient function and clinical efficacy are distinct endpoints. APC, antigen-presenting cell; CAF, cancer-associated fibroblast; CAR-T, chimeric antigen receptor T cell; cDC1, conventional type 1 dendritic cell; GPX4, glutathione peroxidase 4; IDH2, isocitrate dehydrogenase 2; LDH, lactate dehydrogenase; MCT11, monocarboxylate transporter 11; NAD, nicotinamide adenine dinucleotide; NAMPT, nicotinamide phosphoribosyltransferase; P4HA1, prolyl 4-hydroxylase subunit alpha 1; PHGDH, phosphoglycerate dehydrogenase; PKM2, pyruvate kinase M2; STING, stimulator of interferon genes.

CD73 inhibition has produced mixed findings across clinical settings. A first-in-human study of oleclumab, alone or with durvalumab (NCT02503774), enrolled 192 patients and reported manageable safety and evidence of CD73 target engagement. Objective response rates (ORRs) in the colorectal, pancreatic and EGFR-mutant non-small-cell lung cancer expansion cohorts were 2.4%, 4.8% and 9.5%, respectively; the study did not provide a randomized estimate of survival benefit[159]. In the randomized phase II COAST study (NCT03822351), patients with unresectable stage III non-small-cell lung cancer without progression after concurrent chemoradiotherapy received durvalumab alone or with novel agents. The oleclumab combination showed ORRs of 35.0% versus 23.9%, a difference that was not statistically significant. The PFS HR was 0.59 (95% CI, 0.37–0.93), whereas the OS estimate remained uncertain (HR, 0.69; 95% CI, 0.40–1.20)[160]. This is a phase II efficacy signal, not confirmation of an OS benefit or of an adenosine-based selection strategy.

The PACIFIC-9 protocol extends the post-chemoradiotherapy setting to an international, double-blind, randomized phase III comparison. Patients with unresectable stage III non-small-cell lung cancer and no progression after concurrent

chemoradiotherapy receive durvalumab with oleclumab, monalizumab or placebo (NCT05221840). The primary endpoint is progression-free survival assessed by blinded independent central review[161]. The cited publication describes trial design and provides no phase III efficacy estimate. It therefore supplies the development context for COAST while leaving confirmation of benefit and validation of spatial patient selection as separate questions.

COLUMBIA-1 (NCT04068610) tested durvalumab and oleclumab added to FOLFOX and bevacizumab in previously untreated microsatellite-stable metastatic colorectal cancer. In the 52-patient randomized phase II component, ORR was 61.5% versus 46.2%, without a statistically significant difference; the findings did not support further development of that combination in the studied population[162]. These results should not be reduced to uniform success or failure of CD73 blockade. The trials differed in disease, treatment backbone and design, and none prospectively validated patient selection using a spatial adenosine–recipient-cell biomarker. Future studies can test such selection alongside drug exposure, target engagement and conventional clinical outcomes, rather than treating it as an explanation already established by these trials.

6.2 Defining and validating spatial biomarkers

Candidate biomarkers may combine a measured analyte or physiological field with the location of a source and susceptible recipient. GLUT1-positive TAM–$CD8^+$ T cell segregation and experimental peri-necrotic adenosine maps illustrate different levels of evidence for this approach[26, 91]. A clinical assay must specify the tissue site, platform, cell markers, segmentation method, spatial metric, minimum evaluable area and rules for necrosis and missing tissue. Distances and overlap fractions are candidate features, not established thresholds. Where a cut point is needed, it should be developed in a training cohort, fixed before testing, and evaluated in an independent cohort with reproducibility across blocks, observers and centers[163, 164].

Validation should determine whether the spatial feature adds information beyond PD-L1, tumor mutational burden, cell density or an appropriate clinical model. A prognostic association is insufficient for treatment selection: a predictive claim requires evidence that treatment effect differs according to the biomarker, ideally within a prospective randomized design[164]. Routine FFPE-based assays may provide an accessible first layer, with direct metabolite or physiological validation in a material-rich subset. The sampling strategy must remain feasible for the intended clinical population rather than requiring repeated multiregion biopsies from every patient. A negative result should be interpretable in terms of assay performance, tissue coverage, drug exposure and competing biology, not automatically labeled absence of the mechanism.

Regulatory development begins with a specified context of use: the population, specimen and decision supported by the assay. An exploratory regional pharmacodynamic readout, a biomarker used for trial enrichment and a test essential to treatment selection carry different evidentiary demands. For biomarker use in drug development, the US Food and Drug Administration (FDA) qualification framework links the supporting evidence to a specified context of use[165]. Qualification does not itself authorize a diagnostic device. If a spatial test becomes essential to the safe and effective use of a therapy, companion-diagnostic development is a separate pathway that generally proceeds with the therapeutic product[166]. Tissue processing, segmentation and algorithm versions, repeatability, interlaboratory reproducibility and a locked decision rule should accompany clinical validation. These principles provide a development route for candidate spatial assays rather than evidence that a metabolic-territory classifier has already met it.

6.3 Regional and cell-selective interventions

The intervention should address the demonstrated limiting step. For poor access, vascular or stromal treatment can be evaluated through connected perfusion, viable hypoxic fraction, matrix traversal and lymphocyte entry. Endothelial STING and PHGDH studies support this logic in preclinical settings[13, 14, 150], while CAF studies show why selective modulation may be preferable to depletion of all fibroblasts[17, 23, 90]. Reduced vessel or stromal abundance alone is not evidence of restored access. Preservation of APC-rich structures and increased contact with malignant cells are more relevant functional endpoints.

For infiltrated but dysfunctional tissue, source-directed and recipient-directed interventions impose different safety and pharmacodynamic requirements. LDH inhibition can redistribute glucose uptake between tumor and immune cells in models[49], but systemic treatment also reaches activated immune cells with glycolytic requirements. Tumor drug exposure, LDH inhibition, regional lactate and pH, and lineage-specific glucose use should therefore be assessed together. MCT11 blockade acts on lactate uptake in exhausted T cells[44]; its therapeutic window depends on cell-state selectivity, expression in other tissues and reagent specificity. Changes in target-cell uptake and function, supported by target-deficient or other specificity controls, are more

informative than total tissue lactate alone. Tumor SLC43A2 targeting should similarly be distinguished from systemic methionine restriction, with preservation of recipient T cell methionine uptake and methyl-donor metabolism included in the assessment[68].

Lithium-mediated routing of lactic acid toward T cell mitochondrial metabolism is another preclinical approach[167]. Its systemic use requires serum exposure, renal function, fluid and electrolyte status, interacting medicines and neurological toxicity to be considered; the established lithium label emphasizes concentration-related toxicity[168]. Prior use in another indication does not establish an effective or safe tumor-immunity regimen. CD73 glycosylation and stability[169, 170], extracellular GPX4–ZP3 signaling[21], tumor-cell dihydroorotate dehydrogenase (DHODH)-dependent macropinocytosis[171] and fat mass and obesity-associated protein (FTO)-related glycolysis[172] offer other experimental targets. Each requires its own demonstration of target engagement, recipient functional benefit and preservation of immune populations sharing the pathway.

Metabolic support of therapeutic lymphocytes should likewise be assessed at the level of the specific modification. Pyruvate kinase M2 (PKM2) activation and prolyl 4-hydroxylase subunit alpha 1 (P4HA1) targeting improved T cell function or progenitor-associated responses in models[173, 174]. Stem-like T cell properties have clinical associations with adoptive therapy outcome[175], but that association does not validate every metabolic engineering strategy. β-Hydroxybutyrate support, restoration of nicotinamide adenine dinucleotide (NAD) metabolism, and mitochondrial isocitrate dehydrogenase modulation provide additional experimental approaches[176, 177, 178]. IL-10-based reprogramming, interference with LARP4 or Meteorin-like signaling, and FOXP3 expression in CAR-T cells address different aspects of persistence and fitness[31, 140, 179, 180]. Testing should follow sequential hypoxia, acidity, nutrient restriction, matrix migration and repeated target contact, with recovery and sustained killing measured alongside expansion.

6.4 Delivery and treatment sequence

Treatment sequence can be tested against the specific barrier suggested by a tumor model. In glioblastoma, endothelial PHGDH-dependent metabolism has been linked experimentally to abnormal vessels, hypoxia and CAR-T resistance[14]. A comparison of endothelial conditioning before CAR-T infusion with simultaneous treatment could test whether improved perfusion and lower viable-tissue hypoxia precede increased CAR-T entry and tumor-cell contact. If target engagement occurs without improved access, the proposed vascular explanation for that sequence would be weakened. In pancreatic cancer, tumor-cell SLC4A4 inhibition reduced extracellular acidosis and improved antitumor immunity in models[34]. Here, a short pH-correcting lead-in followed by checkpoint blockade could be compared with concurrent treatment, using early extracellular pH and resident $CD8^+$ T cell function as readouts. Failure to restore function despite pH correction would implicate persistent injury or another constraint. These timing comparisons are proposed experiments based on the respective mechanisms, rather than established clinical regimens. Accordingly, any sequencing strategy should be conditioned on tumor type, anatomical site and a measured dominant metabolic barrier rather than applied as a universal schedule; transcript-defined metabolic subtypes should not be used for treatment selection unless they are linked to a reproducible regional chemical or functional phenotype.

Anatomical site constrains delivery as well as metabolism. Liver metastases may involve resident myeloid and stromal programs, while brain lesions differ in vascular permeability and local lipid conditions[58, 115, 117]. Intratumoral injection or a local depot can be tested in accessible lesions, with measurement of viable-tissue coverage, retention and systemic leakage. Heterogeneous distribution and untreated distant disease remain limitations. Tumor-activated prodrugs, targeted carriers and cell-restricted engineering are additional delivery hypotheses whose selectivity must be demonstrated experimentally. Hypoxia-activated or vascularly delivered agents still need access to viable tissue; necrotic tissue may have little drug delivery. Spatial multi-omics and longitudinal observations can nominate regions and timing hypotheses[114, 132, 134, 181], but measured pharmacokinetics and tissue effects determine whether a proposed approach merits prospective testing.

6.5 Longitudinal pharmacodynamics and metabolic niche substitution

An early clinical window or dose-escalation study can separate regional delivery, target engagement and immune recovery. When feasible, sampling should include baseline, the end of a metabolic-agent lead-in, an early combination-treatment time point and residual or progressing tissue. The lead-in should be justified by pharmacokinetics and the time needed for a prespecified tissue effect rather than by an arbitrary

common duration. A concurrent-treatment comparator helps test whether conditioning adds benefit. For an accessible tumor scheduled for resection, an agent with sufficient prior safety data could be evaluated in a short preoperative window without delaying surgery, pairing a baseline core with mapped resection samples. Initial objectives would include safety and regional pharmacodynamics, with drug exposure, target modulation and coverage of viable tissue assessed together. Combination testing would follow acceptable tolerability and the prespecified tissue effect. Regional drug concentration and pathway inhibition establish delivery and engagement; calibrated chemistry, cell-specific uptake and functional assays establish downstream effects[110, 118, 119]. Perfusion and access remain relevant for vascular treatment[10, 11, 13, 14], while cell therapy requires regional persistence and malignant-cell contact[149]. Imaging and molecular assays can extend longitudinal coverage, subject to their resolution and sampling limits[132, 154, 155].

Metabolic niche substitution denotes loss of a previously dominant suppressive influence, supported by target-engagement evidence, followed by a different metabolic process that maintains local immune dysfunction (Table 1). Longitudinal analysis should measure the original target analyte, the candidate compensatory process, viable tumor, immune composition and, where possible, clonal identity in comparable regions. Inadequate penetration, untreated tissue and shifts in cell proportions must be distinguished from a newly dominant dependency. Baseline and treatment-associated cellular trajectories in TNBC provide a precedent for this comparison[114], but do not themselves prove metabolic substitution. Increased expression of another pathway is a candidate adaptation until its chemistry and functional contribution are demonstrated.

Functional testing is needed to link the new process to residual suppression. In a matched slice or experimental model, blocking the candidate alternative should restore immune activity after the original pathway has been inhibited. For example, the emergence of an alternative inhibitory pathway after relief of lactate-associated stress is a testable possibility, not a fixed sequence established in patients. The clinical value of a regional pharmacodynamic feature must then be assessed against outcome and established biomarkers. TLS maturity can be recorded as an immune-structural endpoint, while its unmeasured metabolic support should remain separate from a direct metabolic response.

7. Research priorities

Priority 1 is to establish source-recipient causality at defined interfaces. GLUT1-positive TAM interfaces offer a concrete test of whether metabolic geography contributes beyond cell abundance. Human spatial segregation and macrophage-specific SLC2A1 perturbation in models already link macrophage metabolism to T cell distribution[91]. The missing step is a regional connection between macrophage substrate use and the function of nearby T cells. Paired glucose-uptake measurements, extracellular substrate assessment and live-cell tracking could test whether distance from the interface predicts migration or killing after accounting for macrophage and T cell density, perfusion and matrix structure. If selective perturbation changes local chemistry and restores interface crossing before cell proportions change, it would support this mechanism. If function improves only with altered chemokine or matrix organization while substrate exposure remains unchanged, a glucose-competition explanation would lose support even though the macrophage-dependent barrier remains biologically relevant.

Priority 2 is to determine whether organized immune niches have reproducible chemical support beyond their cellular architecture. TLS provide a complementary test because their structural and clinical associations are stronger than evidence for protected nutrient supply[99, 100]. Comparing mature TLS with nearby viable tissue of similar cellular density would establish whether oxygen, lactate or amino-acid conditions differ reproducibly. The spatial metabolic hypothesis predicts that a measured chemical feature explains local priming or expansion beyond TLS maturity, vascularity and B/T-cell composition. A substrate perturbation that alters function while preserving architecture would strengthen that interpretation. Conversely, the absence of a reproducible chemical difference, together with no functional dependence on the candidate substrate under adequately controlled conditions, would favor a structural explanation for the observed association. These outcomes would refine the interpretation of TLS without diminishing their value as immune-organizational biomarkers.

Priority 3 is to test whether exposure history and regional metrics add information beyond current state and simpler biomarkers. Exposure history can be tested independently of these spatial comparisons. Early methionine restriction produced later T cell impairment despite substrate restoration in experimental systems[137]. Cells exposed to the same current chemistry can therefore be compared after different defined exposure histories, controlling

differentiation state and selective survival. Persistence of a functional difference would support a contribution from earlier stress; equivalent recovery would weaken that explanation within the tested time window. For clinical translation, any regional metric must also improve prediction beyond cell density, tissue composition, bulk metabolic measurements and an appropriate clinical model. Spatially constrained permutation tests can assess whether the observed arrangement carries information beyond these covariates, while independent cohorts and treatment-interaction analyses determine whether that information predicts differential treatment benefit.

Histology-based prediction may enable scalable validation in routine clinical archives. Histology-based virtual spatial proteomics has produced predicted protein maps and clinically associated tissue features in lung cancer[155], while a pan-cancer TLS study predicted maturation from H&E images[101]. These outputs concern protein expression or architecture, not direct lactate, oxygen or amino-acid concentrations. Virtual metabolomics remains a direction requiring paired chemical training and independent validation. Data should be divided by patient and center rather than by image patch, with assessment of staining and scanner variation, treatment-associated distribution shifts and uncertainty. The most tractable initial targets are reproducible structural features such as TLS maturity, tumor–immune separation and stromal interfaces; their relationship to metabolism must then be established rather than assumed.

8. Conclusions

Spatial metabolic organization links local substrate supply, cellular interactions and exposure history to antitumor immune function. Physicochemical fields and cell-organized niches provide complementary descriptions of this heterogeneity, while intercellular mechanisms explain how particular populations influence their neighbors. The next step is to identify regional measurements that explain functional differences beyond cell abundance and bulk metabolism, then test their contribution through selective perturbation and recovery assays. Clinical studies of pathway inhibition establish the activity and limitations of specific regimens; prospective studies must determine whether spatial measurements improve treatment selection. Together, these approaches can connect tissue organization to persistent regional barriers while preserving the immune niches needed for sustained tumor control.

Abbreviations

1-MNA: 1-methylnicotinamide; A2AR: adenosine A2A receptor; AARS1: alanyl-tRNA synthetase 1; ACAT1: acetyl-CoA acetyltransferase 1; ACOD1: aconitate decarboxylase 1; AhR: aryl hydrocarbon receptor; APC: antigen-presenting cell; ATF4: activating transcription factor 4; ATF6: activating transcription factor 6; ATP: adenosine triphosphate; CAF: cancer-associated fibroblast; CAR-NK: chimeric antigen receptor-engineered natural killer cell; CAR-T: chimeric antigen receptor T cell; CD36: cluster of differentiation 36; CD39: ectonucleoside triphosphate diphosphohydrolase 1; CD4: cluster of differentiation 4; CD40: cluster of differentiation 40; CD73: ecto-5′-nucleotidase; CD8: cluster of differentiation 8; cDC1: conventional type 1 dendritic cell; CI: confidence interval; CRC: colorectal cancer; CRISPR: clustered regularly interspaced short palindromic repeats; CXCL12: C-X-C motif chemokine ligand 12; DC: dendritic cell; DESI: desorption electrospray ionization; DHODH: dihydroorotate dehydrogenase; DON: 6-diazo-5-oxo-L-norleucine; EGR1: early growth response 1; eNAMPT: extracellular nicotinamide phosphoribosyltransferase; ER: endoplasmic reticulum; EV: extracellular vesicle; FDA: Food and Drug Administration; FFPE: formalin-fixed paraffin-embedded; FGF21: fibroblast growth factor 21; FLCN: folliculin; FOLFOX: folinic acid, fluorouracil and oxaliplatin; FOXP3: forkhead box P3; FRET: Förster resonance energy transfer; FTO: fat mass and obesity-associated protein; GLUT1: glucose transporter 1; GPX4: glutathione peroxidase 4; H&E: hematoxylin and eosin; HEV: high endothelial venule; HIF: hypoxia-inducible factor; HIF-1α: hypoxia-inducible factor 1-alpha; HR: hazard ratio; IDO1: indoleamine 2,3-dioxygenase 1; IF: immunofluorescence; IHC: immunohistochemistry; IL-10: interleukin 10; ILC: innate lymphoid cell; ILC2: type 2 innate lymphoid cell; IRE1α: inositol-requiring enzyme 1 alpha; IRG1: immune-responsive gene 1; ISR: integrated stress response; LARP4: La-related protein 4; LDH: lactate dehydrogenase; MALDI: matrix-assisted laser desorption/ionization; MCT: monocarboxylate transporter; MCT1: monocarboxylate transporter 1; MCT11: monocarboxylate transporter 11; MCT4: monocarboxylate transporter 4; mregDC: mature dendritic cell enriched in immunoregulatory molecules; MRI: magnetic resonance imaging; MSI: mass spectrometry imaging; MSS: microsatellite stable; mtDNA: mitochondrial DNA; NAD: nicotinamide adenine dinucleotide; NAM: nicotinamide; NAMPT: nicotinamide phosphoribosyltransferase; NICD: Notch intracellular domain; NK: natural killer cell; NNMT: nicotinamide N-methyltransferase; NSCLC: non-small-cell lung cancer; ORR: objective response rate; OS: overall

survival; P4HA1: prolyl 4-hydroxylase subunit alpha 1; PD-1: programmed cell death protein 1; PD-L1: programmed death-ligand 1; PDAC: pancreatic ductal adenocarcinoma; PERK: protein kinase R-like endoplasmic reticulum kinase; PET: positron emission tomography; PFS: progression-free survival; PHGDH: phosphoglycerate dehydrogenase; PKM2: pyruvate kinase M2; RNA: ribonucleic acid; RORγ: retinoic acid receptor-related orphan receptor gamma; SIMS: secondary ion mass spectrometry; SIRT1: sirtuin 1; spFBA: spatial flux balance analysis; STING: stimulator of interferon genes; TAM: tumor-associated macrophage; TCF-1: T cell factor 1; TFEB: transcription factor EB; TGF-β: transforming growth factor beta; Th2: type 2 helper T cell; TIL: tumor-infiltrating lymphocyte; TLS: tertiary lymphoid structure; TME: tumor microenvironment; TNBC: triple-negative breast cancer; TPEX: progenitor-exhausted $CD8^+$ T cell; Treg: regulatory T cell; XBP1: X-box binding protein 1; ZP3: zona pellucida glycoprotein 3.

Acknowledgements

ChatGPT (OpenAI) was used for preliminary English-language editing. The manuscript was subsequently professionally edited by Bullet Edits to further improve the quality of language. The authors reviewed the final text and take full responsibility for the content.

Funding

This work was supported by the Natural Science Foundation of Fujian Province (No. 2026J001185) to Dr. Xin Yu, the National Natural Science Foundation of China (No. 82372780) to Dr. Qi Wu, and the Taikang Healthcare Youth Medical Research Fund (No. 2023005) to Dr. Juanjuan Li.

Authorship contribution statement

Xin Yu: Writing – original draft, Visualization, Investigation, Conceptualization, Funding acquisition. Wenge Li: Writing – original draft, Visualization, Investigation, Conceptualization. Qi Wu: Writing – review & editing, Supervision, Project administration, Funding acquisition, Conceptualization. Juanjuan Li: Writing – review & editing, Supervision, Project administration, Funding acquisition, Conceptualization.

Competing Interests

The authors have declared that no competing interest exists.

References

1. Hanahan D. Hallmarks of cancer: new dimensions. Cancer Discov. 2022; 12: 31–46. doi:10.1158/2159-8290.cd-21-1059.
2. Pavlova NN, Thompson CB. The emerging hallmarks of cancer metabolism. Cell Metab. 2016; 23: 27–47. doi:10.1016/j.cmet.2015.12.006.
3. Buck MD, Sowell RT, Kaech SM, Pearce EL. Metabolic instruction of immunity. Cell. 2017; 169: 570–86. doi:10.1016/j.cell.2017.04.004.
4. Leone RD, Powell JD. Metabolism of immune cells in cancer. Nat Rev Cancer. 2020; 20: 516–31. doi:10.1038/s41568-020-0273-y.
5. DePeaux K, Delgoffe GM. Metabolic barriers to cancer immunotherapy. Nat Rev Immunol. 2021; 21: 785–97. doi:10.1038/s41577-021-00541-y.
6. Reinfeld BI, Madden MZ, Wolf MM, Chytil A, Bader JE, Patterson AR, et al. Cell-programmed nutrient partitioning in the tumour microenvironment. Nature. 2021; 593: 282–8. doi:10.1038/s41586-021-03442-1.
7. Sullivan MR, Danai LV, Lewis CA, Chan SH, Gui DY, Kunchok T, et al. Quantification of microenvironmental metabolites in murine cancers reveals determinants of tumor nutrient availability. Elife. 2019; 8: e44235. doi:10.7554/elife.44235.
8. Hartmann FJ. Spatial immunometabolism: integrating technologies to decode cellular metabolism in tissues. Eur J Immunol. 2025; 55: e70094. doi:10.1002/eji.70094.
9. Demicco M, Liu X-Z, Leithner K, Fendt S-M. Metabolic heterogeneity in cancer. Nat Metab. 2024; 6: 18–38. doi:10.1038/s42255-023-00963-z.
10. Jain RK. Antiangiogenesis strategies revisited: from starving tumors to alleviating hypoxia. Cancer Cell. 2014; 26: 605–22. doi:10.1016/j.ccell.2014.10.006.
11. Fukumura D, Kloepper J, Amoozgar Z, Duda DG, Jain RK. Enhancing cancer immunotherapy using antiangiogenics: opportunities and challenges. Nat Rev Clin Oncol. 2018; 15: 325–40. doi:10.1038/nrclinonc.2018.29.
12. Han M, Bushong EA, Segawa M, Tiard A, Wong A, Brady MR, et al. Spatial mapping of mitochondrial networks and bioenergetics in lung cancer. Nature. 2023; 615: 712–9. doi:10.1038/s41586-023-05793-3.
13. Lv H, Zong Q, Chen C, Lv G, Xiang W, Xing F, et al. TET2-mediated tumor cGAS triggers endothelial STING activation to regulate vasculature remodeling and anti-tumor immunity in liver cancer. Nat Commun. 2024; 15: 6. doi:10.1038/s41467-023-43743-9.
14. Zhang D, Li AM, Hu G, Huang M, Yang F, Zhang L, et al. PHGDH-mediated endothelial metabolism drives glioblastoma resistance to chimeric antigen receptor T cell immunotherapy. Cell Metab. 2023; 35: 517-534.e8. doi:10.1016/j.cmet.2023.01.010.
15. Maspero D, Marteletto G, Lapi F, Galuzzi BG, Ruano I, Vandenbosch B, et al. Spatial FBA reveals heterogeneous warburg niches in renal tumors and lactate consumption in colorectal cancer. NPJ Syst Biol Appl. 2026; 12: 32. doi:10.1038/s41540-026-00654-x.
16. Mansouri S, Hesami G, Ambikan A, Karger A, Klatt S, Neogi U, et al. IRG1/itaconate rewires macrophage and lung tumor metabolism through G6PD inhibition. Cell Metab. 2026; 38: 1460-1477.e8. doi:10.1016/j.cmet.2026.05.005.
17. Ma Z, Wang Y, Wang W, Sun W, Wang R, Ding X, et al. Lipid oxidation reprogramming in cancer-associated fibroblasts enhances CD8+ T cell cytotoxicity and therapeutic response. Cancer Cell. 2026; 44: 743-759.e8. doi:10.1016/j.ccell.2026.01.012.
18. Bader JE, Wolf MM, Lupica-Tondo GL, Madden MZ, Reinfeld BI, Arner EN, et al. Obesity induces PD-1 on macrophages to suppress anti-tumour immunity. Nature. 2024; 630: 968–75. doi:10.1038/s41586-024-07529-3.
19. Ikeda H, Kawase K, Nishi T, Watanabe T, Takenaga K, Inozume T, et al. Immune evasion through mitochondrial transfer in the tumour microenvironment. Nature. 2025; 638: 225–36. doi:10.1038/s41586-024-08439-0.
20. Jiang Y, Wang Y, Chen G, Sun F, Wu Q, Huang Q, et al. Nicotinamide metabolism face-off between macrophages and fibroblasts manipulates the microenvironment in gastric cancer. Cell Metab. 2024; 36: 1806-1822.e11. doi:10.1016/j.cmet.2024.05.013.
21. Liu J, Cai X, Lin J, Zhang Z, Zhou Q, Zhang X, et al. Extracellular GPX4 impairs antitumor immunity via dendritic ZP3 receptors. Cell. 2026; 189: 1056-1073.e24. doi:10.1016/j.cell.2025.12.002.
22. Liu Y, Sinjab A, Min J, Han G, Paradiso F, Zhang Y, et al. Conserved spatial subtypes and cellular neighborhoods of cancer-associated fibroblasts revealed by single-cell spatial multi-omics. Cancer Cell. 2025; 43: 905-924.e6. doi:10.1016/j.ccell.2025.03.004.
23. Broz MT, Ko EY, Ishaya K, Xiao J, De Simone M, Hoi XP, et al. Metabolic targeting of cancer associated fibroblasts overcomes T-cell exclusion and chemoresistance in soft-tissue sarcomas. Nat Commun. 2024; 15: 2498. doi:10.1038/s41467-024-46504-4.
24. Worsley CM, Veale RB, Mayne ES. The acidic tumour microenvironment: manipulating the immune response to elicit escape. Hum Immunol. 2022; 83: 399–408. doi:10.1016/j.humimm.2022.01.014.
25. Alicea Pauneto CDM, Riesenberg BP, Gandy EJ, Kennedy AS, Clutton GT, Hem JW, et al. Intra-tumoral hypoxia promotes CD8+ T cell dysfunction via chronic activation of integrated stress response transcription factor ATF4. Immunity. 2025; 58: 2489-2504.e8. doi:10.1016/j.immuni.2025.09.003.
26. Graziano V, Dannhorn A, Hulme H, Williamson K, Buckley H, Karim SA, et al. Defining the spatial distribution of extracellular adenosine revealed a myeloid-dependent immunosuppressive microenvironment in pancreatic ductal adenocarcinoma. J Immunother Cancer. 2023; 11: e006457. doi:10.1136/jitc-2022-006457.
27. Vignali PDA, DePeaux K, Watson MJ, Ye C, Ford BR, Lontos K, et al. Hypoxia drives CD39-dependent suppressor function in exhausted T cells to limit

antitumor immunity. Nat Immunol. 2023; 24: 267–79. doi:10.1038/s41590-022-01379-9.
28. Chang T-G, Friedman J, Clavijo PE, Robbins Y, Craveiro M, Huynh A, et al. Hypoxia-induced EGR1 remodels neutrophils to suppress antitumor immunity. Sci Immunol. 2025; 10: eadz2273. doi:10.1126/sciimmunol.adz2273.
29. Ugolini A, De Leo A, Yu X, Scirocchi F, Liu X, Peixoto B, et al. Functional reprogramming of neutrophils within the brain tumor microenvironment by hypoxia-driven histone lactylation. Cancer Discov. 2025; 15: 1270–96. doi:10.1158/2159-8290.cd-24-1056.
30. Bossowski JP, Pillai R, Kilian J, Wong Lau A, Nakamura M, Rashidfarrokhi A, et al. The integrated stress response promotes immune evasion through lipocalin 2. Nature. 2026; 652: 1329–38. doi:10.1038/s41586-026-10143-0.
31. Liu Y, Ni H, Li J, Yang J, Sekielyk I, Snow BE, et al. LARP4-mediated hypertranslation drives T cell dysfunction in tumors. Nat Immunol. 2025; 26: 1488–500. doi:10.1038/s41590-025-02232-5.
32. Wu H, Zhao X, Hochrein SM, Eckstein M, Gubert GF, Knöpper K, et al. Mitochondrial dysfunction promotes the transition of precursor to terminally exhausted T cells through HIF-1α-mediated glycolytic reprogramming. Nat Commun. 2023; 14: 6858. doi:10.1038/s41467-023-42634-3.
33. Cheng H, Qiu Y, Xu Y, Chen L, Ma K, Tao M, et al. Extracellular acidosis restricts one-carbon metabolism and preserves T cell stemness. Nat Metab. 2023; 5: 314–30. doi:10.1038/s42255-022-00730-6.
34. Cappellesso F, Orban M-P, Shirgaonkar N, Berardi E, Serneels J, Neveu M-A, et al. Targeting the bicarbonate transporter SLC4A4 overcomes immunosuppression and immunotherapy resistance in pancreatic cancer. Nat Cancer. 2022; 3: 1464–83. doi:10.1038/s43018-022-00470-2.
35. Cubillos-Ruiz JR, Bettigole SE, Glimcher LH. Tumorigenic and immunosuppressive effects of endoplasmic reticulum stress in cancer. Cell. 2017; 168: 692–706. doi:10.1016/j.cell.2016.12.004.
36. Song M, Sandoval TA, Chae C-S, Chopra S, Tan C, Rutkowski MR, et al. IRE1α-XBP1 controls T cell function in ovarian cancer by regulating mitochondrial activity. Nature. 2018; 562: 423–8. doi:10.1038/s41586-018-0597-x.
37. Mandula JK, Chang S, Mohamed E, Jimenez R, Sierra-Mondragon RA, Chang DC, et al. Ablation of the endoplasmic reticulum stress kinase PERK induces paraptosis and type I interferon to promote anti-tumor T cell responses. Cancer Cell. 2022; 40: 1145-1160.e9. doi:10.1016/j.ccell.2022.08.016.
38. Eil R, Vodnala SK, Clever D, Klebanoff CA, Sukumar M, Pan JH, et al. Ionic immune suppression within the tumour microenvironment limits T cell effector function. Nature. 2016; 537: 539–43. doi:10.1038/nature19364.
39. Wong BHS, Poh ZS, Wei JTC, Amuthavalli K, Ho YS, Chen S, et al. High extracellular K+ skews T-cell differentiation towards tumour promoting Th2 and Treg subsets. Eur J Immunol. 2025; 55: e202451440. doi:10.1002/eji.202451440.
40. Apetoh L, Ghiringhelli F, Tesniere A, Obeid M, Ortiz C, Criollo A, et al. Toll-like receptor 4-dependent contribution of the immune system to anticancer chemotherapy and radiotherapy. Nat Med. 2007; 13: 1050–1059. doi:10.1038/nm1622.
41. Seifert L, Werba G, Tiwari S, Giao Ly NN, Alothman S, Alqunaibit D, et al. The necrosome promotes pancreatic oncogenesis via CXCL1 and Mincle-induced immune suppression. Nature. 2016; 532: 245–249. doi:10.1038/nature17403.
42. Scirgolea C, Sottile R, De Luca M, Susana A, Carnevale S, Puccio S, et al. NaCl enhances CD8+ T cell effector functions in cancer immunotherapy. Nat Immunol. 2024; 25: 1845–57. doi:10.1038/s41590-024-01923-9.
43. Brand A, Singer K, Koehl GE, Kolitzus M, Schoenhammer G, Thiel A, et al. LDHA-Associated Lactic Acid Production Blunts Tumor Immunosurveillance by T and NK Cells. Cell Metab. 2016; 24: 657–71. doi:10.1016/j.cmet.2016.08.011.
44. Peralta RM, Xie B, Lontos K, Nieves-Rosado H, Spahr K, Joshi S, et al. Dysfunction of exhausted T cells is enforced by MCT11-mediated lactate metabolism. Nat Immunol. 2024; 25: 2297–307. doi:10.1038/s41590-024-01999-3.
45. Kumagai S, Koyama S, Itahashi K, Tanegashima T, Lin Y-T, Togashi Y, et al. Lactic acid promotes PD-1 expression in regulatory T cells in highly glycolytic tumor microenvironments. Cancer Cell. 2022; 40: 201-218.e9. doi:10.1016/j.ccell.2022.01.001.
46. Watson MJ, Vignali PDA, Mullett SJ, Overacre-Delgoffe AE, Peralta RM, Grebinoski S, et al. Metabolic support of tumour-infiltrating regulatory T cells by lactic acid. Nature. 2021; 591: 645–51. doi:10.1038/s41586-020-03045-2.
47. Angelin A, Gil-de-Gómez L, Dahiya S, Jiao J, Guo L, Levine MH, et al. Foxp3 reprograms T cell metabolism to function in low-glucose, high-lactate environments. Cell Metab. 2017; 25: 1282-1293.e7. doi:10.1016/j.cmet.2016.12.018.
48. Feng Q, Liu Z, Yu X, Huang T, Chen J, Wang J, et al. Lactate increases stemness of CD8+ T cells to augment anti-tumor immunity. Nat Commun. 2022; 13: 4981. doi:10.1038/s41467-022-32521-8.
49. Verma S, Budhu S, Serganova I, Dong L, Mangarin LM, Khan JF, et al. Pharmacologic LDH inhibition redirects intratumoral glucose uptake and improves antitumor immunity in solid tumor models. J Clin Invest. 2024; 134: e177606. doi:10.1172/jci177606.
50. Sun K, Zhang X, Shi J, Huang J, Wang S, Li X, et al. Elevated protein lactylation promotes immunosuppressive microenvironment and therapeutic resistance in pancreatic ductal adenocarcinoma. J Clin Invest. 2025; 135: e187024. doi:10.1172/jci187024.
51. Yang J, Yu X, Xiao M, Xu H, Tan Z, Lei Y, et al. Histone lactylation-driven feedback loop modulates cholesterol-linked immunosuppression in pancreatic cancer. Gut. 2025; 74: 1859–72. doi:10.1136/gutjnl-2024-334361.
52. Wang Y, Li F, Li J, Huang T, Huang T, Zhang N, et al. AARS1 promotes tumor progression and immune evasion via ATF6 lactylation-mediated tryptophan metabolism in hepatocellular carcinoma. Cell Metab. 2026; 38: 1702-1721.e11. doi:10.1016/j.cmet.2026.06.003.
53. Ma X, Xiao L, Liu L, Ye L, Su P, Bi E, et al. CD36-mediated ferroptosis dampens intratumoral CD8+ T cell effector function and impairs their antitumor ability. Cell Metab. 2021; 33: 1001-1012.e5. doi:10.1016/j.cmet.2021.02.015.
54. Xu S, Chaudhary O, Rodríguez-Morales P, Sun X, Chen D, Zappasodi R, et al. Uptake of oxidized lipids by the scavenger receptor CD36 promotes lipid peroxidation and dysfunction in CD8+ T cells in tumors. Immunity. 2021; 54: 1561-1577.e7. doi:10.1016/j.immuni.2021.05.003.
55. Nieman KM, Kenny HA, Penicka CV, Ladanyi A, Buell-Gutbrod R, Zillhardt MR, et al. Adipocytes promote ovarian cancer metastasis and provide energy for rapid tumor growth. Nat Med. 2011; 17: 1498–1503. doi:10.1038/nm.2492.
56. Ugolini A, Tyurin VA, Tyurina YY, Tcyganov EN, Donthireddy L, Kagan VE, et al. Polymorphonuclear myeloid-derived suppressor cells limit antigen cross-presentation by dendritic cells in cancer. JCI Insight. 2020; 5: e138581. doi:10.1172/jci.insight.138581.
57. Yang P, Qin H, Li Y, Xiao A, Zheng E, Zeng H, et al. CD36-mediated metabolic crosstalk between tumor cells and macrophages affects liver metastasis. Nat Commun. 2022; 13: 5782. doi:10.1038/s41467-022-33349-y.
58. Ferraro GB, Ali A, Luengo A, Kodack DP, Deik A, Abbott KL, et al. Fatty acid synthesis is required for breast cancer brain metastasis. Nat Cancer. 2021; 2: 414–28. doi:10.1038/s43018-021-00183-y.
59. Ping Y, Shan J, Qin H, Li F, Qu J, Guo R, et al. PD-1 signaling limits expression of phospholipid phosphatase 1 and promotes intratumoral CD8+ T cell ferroptosis. Immunity. 2024; 57: 2122-2139.e9. doi:10.1016/j.immuni.2024.08.003.
60. Hu C, Qiao W, Li X, Ning Z-K, Liu J, Dalangood S, et al. Tumor-secreted FGF21 acts as an immune suppressor by rewiring cholesterol metabolism of CD8+ T cells. Cell Metab. 2024; 36: 630-647.e8. doi:10.1016/j.cmet.2024.01.005.
61. Yan C, Zheng L, Jiang S, Yang H, Guo J, Jiang L-Y, et al. Exhaustion-associated cholesterol deficiency dampens the cytotoxic arm of antitumor immunity. Cancer Cell. 2023; 41: 1276-1293.e11. doi:10.1016/j.ccell.2023.04.016.
62. Nava Lauson CB, Tiberti S, Corsetto PA, Conte F, Tyagi P, Machwirth M, et al. Linoleic acid potentiates CD8+ T cell metabolic fitness and antitumor immunity. Cell Metab. 2023; 35: 633-650.e9. doi:10.1016/j.cmet.2023.02.013.
63. Bleve A, Incerti M, Consonni FM, Garlatti V, Ballerini G, Pandolfo C, et al. RORγ bridges cancer-driven lipid dysmetabolism and myeloid immunosuppression. Cancer Discov. 2025; 15: 1505–25. doi:10.1158/2159-8290.cd-24-0199.
64. Zhao Y, Liu Z, Liu G, Zhang Y, Liu S, Gan D, et al. Neutrophils resist ferroptosis and promote breast cancer metastasis through aconitate decarboxylase 1. Cell Metab. 2023; 35: 1688-1703.e10. doi:10.1016/j.cmet.2023.09.004.
65. Varanasi SK, Chen D, Liu Y, Johnson MA, Miller CM, Ganguly S, et al. Bile acid synthesis impedes tumor-specific T cell responses during liver cancer. Science. 2025; 387: 192–201. doi:10.1126/science.adl4100.
66. Ni H, Reitman ZJ, Zou W, Akhtar MN, Paul R, Huang M, et al. FLASH radiation reprograms lipid metabolism and macrophage immunity and sensitizes medulloblastoma to CAR-T cell therapy. Nat Cancer. 2025; 6: 460–73. doi:10.1038/s43018-025-00905-6.
67. Lei G, Zhuang L, Gan B. The roles of ferroptosis in cancer: tumor suppression, tumor microenvironment, and therapeutic interventions. Cancer Cell. 2024; 42: 513–34. doi:10.1016/j.ccell.2024.03.011.
68. Bian Y, Li W, Kremer DM, Sajjakulnukit P, Li S, Crespo J, et al. Cancer SLC43A2 alters T cell methionine metabolism and histone methylation. Nature. 2020; 585: 277–82. doi:10.1038/s41586-020-2682-1.
69. Yang Y, Pei T, Liu C, Cao M, Hu X, Yuan J, et al. Glutamine metabolic competition drives immunosuppressive reprogramming of intratumour GPR109A+ myeloid cells to promote liver cancer progression. Gut. 2025; 74: 255–69. doi:10.1136/gutjnl-2024-332429.
70. Xiao Y, Xu Y, Wang H, Yang F, Ding X-H, Fu T, et al. HEBP2-governed glutamine competition between tumor and macrophages dictates immunotherapy efficacy in triple-negative breast cancer. Cell Metab. 2025; 37: 2030-2047.e7. doi:10.1016/j.cmet.2025.08.009.
71. Guo C, You Z, Shi H, Sun Y, Du X, Palacios G, et al. SLC38A2 and glutamine signalling in cDC1s dictate anti-tumour immunity. Nature. 2023; 620: 200–8. doi:10.1038/s41586-023-06299-8.
72. Leone RD, Zhao L, Englert JM, Sun I-M, Oh M-H, Sun I-H, et al. Glutamine blockade induces divergent metabolic programs to overcome tumor immune evasion. Science. 2019; 366: 1013–21. doi:10.1126/science.aav2588.
73. Geiger R, Rieckmann JC, Wolf T, Basso C, Feng Y, Fuhrer T, et al. L-arginine modulates T cell metabolism and enhances survival and anti-tumor activity. Cell. 2016; 167: 829-842.e13. doi:10.1016/j.cell.2016.09.031.
74. Rodriguez PC, Quiceno DG, Zabaleta J, Ortiz B, Zea AH, Piazuelo MB, et al. Arginase I production in the tumor microenvironment by mature myeloid cells inhibits T-cell receptor expression and antigen-specific T-cell responses. Cancer Res. 2004; 64: 5839–49. doi:10.1158/0008-5472.CAN-04-0465.
75. Rowe JH, Elia I, Shahid O, Gaudiano EF, Sifnugel NE, Johnson S, et al. Formate Supplementation Enhances Antitumor CD8+ T-cell Fitness and Efficacy of PD-1 Blockade. Cancer Discov. 2023; 13: 2566–83. doi:10.1158/2159-8290.cd-22-1301.
76. Zhang X-Y, Shi J-B, Jin S-F, Wang R-J, Li M-Y, Zhang Z-Y, et al. Metabolic landscape of head and neck squamous cell carcinoma informs a novel

kynurenine/siglec-15 axis in immune escape. Cancer Commun (Lond). 2024; 44: 670–94. doi:10.1002/cac2.12545.
77. Liu Y, Liu Z, Hu Y, Ling Y, Qing S, Liu Y, et al. Caffeine enhances antitumor T-cell activity by suppressing kynurenine pathway in colorectal cancer. Nat Commun. 2025; 16: 5906. doi:10.1038/s41467-025-60958-0.
78. Bender MJ, McPherson AC, Phelps CM, Pandey SP, Laughlin CR, Shapira JH, et al. Dietary tryptophan metabolite released by intratumoral Lactobacillus reuteri facilitates immune checkpoint inhibitor treatment. Cell. 2023; 186: 1846-1862.e26. doi:10.1016/j.cell.2023.03.011.
79. Campesato LF, Budhu S, Tchaicha J, Weng C-H, Gigoux M, Cohen IJ, et al. Blockade of the AHR restricts a Treg-macrophage suppressive axis induced by L-kynurenine. Nat Commun. 2020; 11: 4011. doi:10.1038/s41467-020-17750-z.
80. Bell HN, Huber AK, Singhal R, Korimerla N, Rebernick RJ, Kumar R, et al. Microenvironmental ammonia enhances T cell exhaustion in colorectal cancer. Cell Metab. 2023; 35: 134-149.e6. doi:10.1016/j.cmet.2022.11.013.
81. Pelka K, Hofree M, Chen JH, Sarkizova S, Pirl JD, Jorgji V, et al. Spatially organized multicellular immune hubs in human colorectal cancer. Cell. 2021; 184: 4734-4752.e20. doi:10.1016/j.cell.2021.08.003.
82. Sorin M, Rezanejad M, Karimi E, Fiset B, Desharnais L, Perus LJM, et al. Single-cell spatial landscapes of the lung tumour immune microenvironment. Nature. 2023; 614: 548–54. doi:10.1038/s41586-022-05672-3.
83. Keren L, Bosse M, Marquez D, Angoshtari R, Jain S, Varma S, et al. A structured tumor-immune microenvironment in triple negative breast cancer revealed by multiplexed ion beam imaging. Cell. 2018; 174: 1373-1387.e19. doi:10.1016/j.cell.2018.08.039.
84. Schürch CM, Bhate SS, Barlow GL, Phillips DJ, Noti L, Zlobec I, et al. Coordinated cellular neighborhoods orchestrate antitumoral immunity at the colorectal cancer invasive front. Cell. 2020; 182: 1341-1359.e19. doi:10.1016/j.cell.2020.07.005.
85. Hua Y, Vella G, Rambow F, Allen E, Antoranz Martinez A, Duhamel M, et al. Cancer immunotherapies transition endothelial cells into HEVs that generate TCF1+ T lymphocyte niches through a feed-forward loop. Cancer Cell. 2022; 40: 1600-1618.e10. doi:10.1016/j.ccell.2022.11.002.
86. Jansen CS, Prokhnevska N, Master VA, Sanda MG, Carlisle JW, Bilen MA, et al. An intra-tumoral niche maintains and differentiates stem-like CD8 T cells. Nature. 2019; 576: 465–70. doi:10.1038/s41586-019-1836-5.
87. Magen A, Hamon P, Fiaschi N, Soong BY, Park MD, Mattiuz R, et al. Intratumoral dendritic cell–CD4+ T helper cell niches enable CD8+ T cell differentiation following PD-1 blockade in hepatocellular carcinoma. Nat Med. 2023; 29: 1389–99. doi:10.1038/s41591-023-02345-0.
88. Chen JH, Nieman LT, Spurrell M, Jorgji V, Elmelech L, Richieri P, et al. Human lung cancer harbors spatially organized stem-immunity hubs associated with response to immunotherapy. Nat Immunol. 2024; 25: 644–58. doi:10.1038/s41590-024-01792-2.
89. Meiser P, Knolle MA, Hirschberger A, de Almeida GP, Bayerl F, Lacher S, et al. A distinct stimulatory cDC1 subpopulation amplifies CD8+ T cell responses in tumors for protective anti-cancer immunity. Cancer Cell. 2023; 41: 1498-1515.e10. doi:10.1016/j.ccell.2023.06.008.
90. Song J, Wei R, Liu C, Zhao Z, Liu X, Wang Y, et al. Antigen-presenting cancer associated fibroblasts enhance antitumor immunity and predict immunotherapy response. Nat Commun. 2025; 16: 2175. doi:10.1038/s41467-025-57465-7.
91. Wang L, Chu H, Chen D, Wei Y, Jia J, Li L, et al. SLC2A1+ tumour-associated macrophages spatially control CD8+ T cell function and drive resistance to immunotherapy in non-small-cell lung cancer. Nat Cell Biol. 2026; 28: 338–48. doi:10.1038/s41556-025-01840-5.
92. Simula L, Fumagalli M, Vimeux L, Rajnpreht I, Icard P, Birsen G, et al. Mitochondrial metabolism sustains CD8+ T cell migration for an efficient infiltration into solid tumors. Nat Commun. 2024; 15: 2203. doi:10.1038/s41467-024-46377-7.
93. Ho P-C, Bihuniak JD, Macintyre AN, Staron M, Liu X, Amezquita R, et al. Phosphoenolpyruvate is a metabolic checkpoint of anti-tumor T cell responses. Cell. 2015; 162: 1217–28. doi:10.1016/j.cell.2015.08.012.
94. Baldominos P, Barbera-Mourelle A, Barreiro O, Huang Y, Wight A, Cho J-W, et al. Quiescent cancer cells resist T cell attack by forming an immunosuppressive niche. Cell. 2022; 185: 1694-1708.e19. doi:10.1016/j.cell.2022.03.033.
95. Marteau V, Nemati N, Handler K, Raju D, Kirchmair A, Rieder D, et al. Single-cell integration and multi-modal profiling reveals phenotypes and spatial organization of neutrophils in colorectal cancer. Cancer Cell. 2026; 44: 146-165.e14. doi:10.1016/j.ccell.2025.12.003.
96. Liu Z, Zhang Z, Zhang Y, Zhou W, Zhang X, Peng C, et al. Spatial transcriptomics reveals that metabolic characteristics define the tumor immunosuppression microenvironment via iCAF transformation in oral squamous cell carcinoma. Int J Oral Sci. 2024; 16: 9. doi:10.1038/s41368-023-00267-8.
97. Zhang Y, Ling L, Murad R, Maganti S, Manceau A, Hetrick HA, et al. Macropinocytosis maintains CAF subtype identity under metabolic stress in pancreatic cancer. Cancer Cell. 2025; 43: 1677-1696.e15. doi:10.1016/j.ccell.2025.06.021.
98. Haist M, Baertsch M-A, Reticker-Flynn NE, Lu G, Kempchen TN, Chu P, et al. Lymph node colonization induces tissue remodeling via immunosuppressive fibroblast-myeloid cell niches supporting metastatic tolerance. Cancer Cell. 2026; 44: 604-623.e9. doi:10.1016/j.ccell.2026.01.003.
99. Cabrita R, Lauss M, Sanna A, Donia M, Skaarup Larsen M, Mitra S, et al. Tertiary lymphoid structures improve immunotherapy and survival in melanoma. Nature. 2020; 577: 561–5. doi:10.1038/s41586-019-1914-8.
100. Helmink BA, Reddy SM, Gao J, Zhang S, Basar R, Thakur R, et al. B cells and tertiary lymphoid structures promote immunotherapy response. Nature. 2020; 577: 549–55. doi:10.1038/s41586-019-1922-8.
101. Cho KS, Liu Y, Pei G, Chen J, Dai Y, Liu Y, et al. Pan-cancer spatial atlas of tertiary lymphoid structures. Science. 2026; 392: eadz2742. doi:10.1126/science.adz2742.
102. Li H, Zhang M-J, Zhang B, Lin W-P, Li S-J, Xiong D, et al. Mature tertiary lymphoid structures evoke intra-tumoral T and B cell responses via progenitor exhausted CD4+ T cells in head and neck cancer. Nat Commun. 2025; 16: 4228. doi:10.1038/s41467-025-59341-w.
103. Liu Y, Ye S-Y, He S, Chi D-M, Wang X-Z, Wen Y-F, et al. Single-cell and spatial transcriptome analyses reveal tertiary lymphoid structures linked to tumour progression and immunotherapy response in nasopharyngeal carcinoma. Nat Commun. 2024; 15: 7713. doi:10.1038/s41467-024-52153-4.
104. Chen C, An M, Zheng H, Pang M, Li Y, Diao X, et al. B cells disrupt tertiary lymphoid structure formation and suppress anti-tumor immunity. Cancer Cell. 2026; 44: 551-566.e17. doi:10.1016/j.ccell.2025.12.011.
105. Jiao M, Guo Y, Zhang H, Wen H, Chen P, Wang Z, et al. ACAT1 regulates tertiary lymphoid structures and correlates with immunotherapy response in non–small cell lung cancer. J Clin Invest. 2025; 135: e181517. doi:10.1172/jci181517.
106. MacFawn IP, Magnon G, Gorecki G, Kunning S, Rashid R, Kaiza ME, et al. The activity of tertiary lymphoid structures in high grade serous ovarian cancer is governed by site, stroma, and cellular interactions. Cancer Cell. 2024; 42: 1864-1881.e5. doi:10.1016/j.ccell.2024.09.007.
107. Dong M, Böpple K, Thiel J, Winkler B, Liang C, Schueler J, et al. Perfusion Air Culture of Precision-Cut Tumor Slices: An Ex Vivo System to Evaluate Individual Drug Response under Controlled Culture Conditions. Cells. 2023; 12: 807. doi:10.3390/cells12050807.
108. Anbaei P, Stevens MG, Ball AG, Bullock TNJ, Pompano RR. Spatially resolved quantification of oxygen consumption rate in ex vivo lymph node slices. Analyst. 2024; 149: 2609–2620. doi:10.1039/d4an00028e.
109. Weltin A, Slotwinski K, Kieninger J, Moser I, Jobst G, Wego M, et al. Cell culture monitoring for drug screening and cancer research: a transparent, microfluidic, multi-sensor microsystem. Lab Chip. 2014; 14: 138–146. doi:10.1039/c3lc50759a.
110. Hu T, Allam M, Cai S, Henderson W, Yueh B, Garipcan A, et al. Single-cell spatial metabolomics with cell-type specific protein profiling for tissue systems biology. Nat Commun. 2023; 14: 8260. doi:10.1038/s41467-023-43917-5.
111. Shen S, Li J, Huo S, Ma M, Zhu X, Rasam S, et al. Parallel, High-Quality Proteomic and Targeted Metabolomic Quantification Using Laser Capture Microdissected Tissues. Anal Chem. 2021; 93: 8711–8718. doi:10.1021/acs.analchem.1c01026.
112. Osorio JC, Knorr DA, Weitzenfeld P, Blanchard L, Yao N, Baez M, et al. Fc-optimized CD40 agonistic antibody elicits tertiary lymphoid structure formation and systemic antitumor immunity in metastatic cancer. Cancer Cell. 2025; 43: 1902-1916.e9. doi:10.1016/j.ccell.2025.07.013.
113. Wang X, Venet D, Lifrange F, Larsimont D, Rediti M, Stenbeck L, et al. Spatial transcriptomics reveals substantial heterogeneity in triple-negative breast cancer with potential clinical implications. Nat Commun. 2024; 15: 10232. doi:10.1038/s41467-024-54145-w.
114. Shiao SL, Gouin KH, Ing N, Ho A, Basho R, Shah A, et al. Single-cell and spatial profiling identify three response trajectories to pembrolizumab and radiation therapy in triple negative breast cancer. Cancer Cell. 2024; 42: 70-84.e8. doi:10.1016/j.ccell.2023.12.012.
115. Sathe A, Mason K, Grimes SM, Zhou Z, Lau BT, Bai X, et al. Colorectal cancer metastases in the liver establish immunosuppressive spatial networking between tumor-associated SPP1+ macrophages and fibroblasts. Clin Cancer Res. 2023; 29: 244–60. doi:10.1158/1078-0432.ccr-22-2041.
116. Shiri AM, Zhang T, Bedke T, Zazara DE, Zhao L, Lücke J, et al. IL-10 dampens antitumor immunity and promotes liver metastasis via PD-L1 induction. J Hepatol. 2024; 80: 634–44. doi:10.1016/j.jhep.2023.12.015.
117. Karimi E, Yu MW, Maritan SM, Perus LJM, Rezanejad M, Sorin M, et al. Single-cell spatial immune landscapes of primary and metastatic brain tumours. Nature. 2023; 614: 555–63. doi:10.1038/s41586-022-05680-3.
118. Wadie B, Stuart L, Rath CM, Drotleff B, Mamedov S, Alexandrov T. METASPACE-ML: context-specific metabolite annotation for imaging mass spectrometry using machine learning. Nat Commun. 2024; 15: 9110. doi:10.1038/s41467-024-52213-9.
119. Buglakova E, Ekelöf M, Schwaiger-Haber M, Schlicker L, Molenaar MR, Shahraz M, et al. Spatial single-cell isotope tracing reveals heterogeneity of de novo fatty acid synthesis in cancer. Nat Metab. 2024; 6: 1695–711. doi:10.1038/s42255-024-01118-4.
120. Shi SR, Key ME, Kalra KL. Antigen retrieval in formalin-fixed, paraffin-embedded tissues: an enhancement method for immunohistochemical staining based on microwave oven heating of tissue sections. J Histochem Cytochem. 1991; 39: 741–748. doi:10.1177/39.6.1709656.
121. Rao A, Barkley D, França GS, Yanai I. Exploring tissue architecture using spatial transcriptomics. Nature. 2021; 596: 211–20. doi:10.1038/s41586-021-03634-9.

122. Lewis SM, Asselin-Labat M-L, Nguyen Q, Berthelet J, Tan X, Wimmer VC, et al. Spatial omics and multiplexed imaging to explore cancer biology. Nat Methods. 2021; 18: 997–1012. doi:10.1038/s41592-021-01203-6.
123. Moses L, Pachter L. Museum of spatial transcriptomics. Nat Methods. 2022; 19: 534–46. doi:10.1038/s41592-022-01409-2.
124. Schott M, León-Periñán D, Splendiani E, Strenger L, Licha JR, Pentimalli TM, et al. Open-ST: high-resolution spatial transcriptomics in 3D. Cell. 2024; 187: 3953-3972.e26. doi:10.1016/j.cell.2024.05.055.
125. Lin J-R, Wang S, Coy S, Chen Y-A, Yapp C, Tyler M, et al. Multiplexed 3D atlas of state transitions and immune interaction in colorectal cancer. Cell. 2023; 186: 363-381.e19. doi:10.1016/j.cell.2022.12.028.
126. Liu X, Tao L, Jiang X, Qu X, Duan W, Yu J, et al. Isoporous membrane mediated imprinting mass spectrometry imaging for spatially-resolved metabolomics and rapid histopathological diagnosis. Small Methods. 2024; 8: e2301644. doi:10.1002/smtd.202301644.
127. Zhu Y, Cai Y, Wang Q, Guo H, Xie Q, Xiang Y, et al. Spatially resolved metabolomic profiling reveals progression-associated metabolic reprogramming in colorectal liver metastasis. Metabolites. 2026; 16: 293. doi:10.3390/metabo16050293.
128. San Martín A, Ceballo S, Ruminot I, Lerchundi R, Frommer WB, Barros LF. A genetically encoded FRET lactate sensor and its use to detect the Warburg effect in single cancer cells. PLoS One. 2013; 8: e57712. doi:10.1371/journal.pone.0057712.
129. Nasu Y, Aggarwal A, Le GNT, Vo CT, Kambe Y, Wang X, et al. Lactate biosensors for spectrally and spatially multiplexed fluorescence imaging. Nat Commun. 2023; 14: 6598. doi:10.1038/s41467-023-42230-5.
130. Miesenböck G, De Angelis DA, Rothman JE. Visualizing secretion and synaptic transmission with pH-sensitive green fluorescent proteins. Nature. 1998; 394: 192–5. doi:10.1038/28190.
131. Buescher JM, Antoniewicz MR, Boros LG, Burgess SC, Brunengraber H, Clish CB, et al. A roadmap for interpreting 13C metabolite labeling patterns from cells. Curr Opin Biotechnol. 2015; 34: 189–201. doi:10.1016/j.copbio.2015.02.003.
132. Meghdadi B, Al-Holou WN, Scott AJ, Mittal A, Liang N, Sravya P, et al. Digital twins for in vivo metabolic flux estimations in patients with brain cancer. Cell Metab. 2026; 38: 228-246.e17. doi:10.1016/j.cmet.2025.10.022.
133. Dhainaut M, Rose SA, Akturk G, Wroblewska A, Nielsen SR, Park ES, et al. Spatial CRISPR genomics identifies regulators of the tumor microenvironment. Cell. 2022; 185: 1223-1239.e20. doi:10.1016/j.cell.2022.02.015.
134. Wu H, Zhang Q, Cao Z, Cao H, Wu M, Fu M, et al. Integrated spatial omics of metabolic reprogramming and the tumor microenvironment in pancreatic cancer. iScience. 2025; 28: 112681. doi:10.1016/j.isci.2025.112681.
135. Sun C, Wang A, Zhou Y, Chen P, Wang X, Huang J, et al. Spatially resolved multi-omics highlights cell-specific metabolic remodeling and interactions in gastric cancer. Nat Commun. 2023; 14: 2692. doi:10.1038/s41467-023-38360-5.
136. Prokhnevska N, Cardenas MA, Valanparambil RM, Sobierajska E, Barwick BG, Jansen C, et al. CD8+ T cell activation in cancer comprises an initial activation phase in lymph nodes followed by effector differentiation within the tumor. Immunity. 2023; 56: 107-124.e5. doi:10.1016/j.immuni.2022.12.002.
137. Sharma P, Guo A, Poudel S, Boada-Romero E, Verbist KC, Palacios G, et al. Early methionine availability attenuates T cell exhaustion. Nat Immunol. 2025; 26: 1384–96. doi:10.1038/s41590-025-02223-6.
138. Yost KE, Satpathy AT, Wells DK, Qi Y, Wang C, Kageyama R, et al. Clonal replacement of tumor-specific T cells following PD-1 blockade. Nat Med. 2019; 25: 1251–9. doi:10.1038/s41591-019-0522-3.
139. O'Flanagan CH, Campbell KR, Zhang AW, Kabeer F, Lim JLP, Biele J, et al. Dissociation of solid tumor tissues with cold active protease for single-cell RNA-seq minimizes conserved collagenase-associated stress responses. Genome Biol. 2019; 20: 210. doi:10.1186/s13059-019-1830-0.
140. Guo Y, Xie Y-Q, Gao M, Zhao Y, Franco F, Wenes M, et al. Metabolic reprogramming of terminally exhausted CD8+ T cells by IL-10 enhances anti-tumor immunity. Nat Immunol. 2021; 22: 746–56. doi:10.1038/s41590-021-00940-2.
141. Chu Y, Dai E, Li Y, Han G, Pei G, Ingram DR, et al. Pan-cancer T cell atlas links a cellular stress response state to immunotherapy resistance. Nat Med. 2023; 29: 1550–62. doi:10.1038/s41591-023-02371-y.
142. Jiang Z, Wang H, Wang X, Duo H, Tao Y, Li J, et al. TMED4 facilitates regulatory T cell suppressive function via ROS homeostasis in tumor and autoimmune mouse models. J Clin Invest. 2025; 135: e179874. doi:10.1172/jci179874.
143. Blidner AG, Bach CA, García PA, Merlo JP, Cagnoni AJ, Bannoud N, et al. Glycosylation-driven programs coordinate immunoregulatory and pro-angiogenic functions of myeloid-derived suppressor cells. Immunity. 2025; 58: 1553-1571.e8. doi:10.1016/j.immuni.2025.04.027.
144. Michelet X, Dyck L, Hogan A, Loftus RM, Duquette D, Wei K, et al. Metabolic reprogramming of natural killer cells in obesity limits antitumor responses. Nat Immunol. 2018; 19: 1330–40. doi:10.1038/s41590-018-0251-7.
145. Biederstädt A, Basar R, Park J-M, Uprety N, Shrestha R, Reyes Silva F, et al. Genome-wide CRISPR screens identify critical targets to enhance CAR-NK cell antitumor potency. Cancer Cell. 2025; 43: 2069-2088.e11. doi:10.1016/j.ccell.2025.07.021.
146. Moral JA, Leung J, Rojas LA, Ruan J, Zhao J, Sethna Z, et al. ILC2s amplify PD-1 blockade by activating tissue-specific cancer immunity. Nature. 2020; 579: 130–5. doi:10.1038/s41586-020-2015-4.
147. Hegde PS, Chen DS. Top 10 challenges in cancer immunotherapy. Immunity. 2020; 52: 17–35. doi:10.1016/j.immuni.2019.12.011.
148. Schoenfeld AJ, Hellmann MD. Acquired resistance to immune checkpoint inhibitors. Cancer Cell. 2020; 37: 443–55. doi:10.1016/j.ccell.2020.03.017.
149. Cascone T, McKenzie JA, Mbofung RM, Punt S, Wang Z, Xu C, et al. Increased tumor glycolysis characterizes immune resistance to adoptive T cell therapy. Cell Metab. 2018; 27: 977-987.e4. doi:10.1016/j.cmet.2018.02.024.
150. Wang-Bishop L, Kimmel BR, Ngwa VM, Madden MZ, Baljon JJ, Florian DC, et al. STING-activating nanoparticles normalize the vascular-immune interface to potentiate cancer immunotherapy. Sci Immunol. 2023; 8: eadd1153. doi:10.1126/sciimmunol.add1153.
151. Li G-Y, Feng Y-Q, Jia Y-F, Wang K-F, Li Y, Zhang S-J, et al. Metformin enhances T lymphocyte anti-tumor immunity by increasing the infiltration via vessel normalization. Eur J Pharmacol. 2023; 944: 175592. doi:10.1016/j.ejphar.2023.175592.
152. Enfield KSS, Colliver E, Lee C, Magness A, Moore DA, Sivakumar M, et al. Spatial architecture of myeloid and T cells orchestrates immune evasion and clinical outcome in lung cancer. Cancer Discov. 2024; 14: 1018–47. doi:10.1158/2159-8290.cd-23-1380.
153. Moldoveanu D, Ramsay L, Lajoie M, Anderson-Trocme L, Lingrand M, Berry D, et al. Spatially mapping the immune landscape of melanoma using imaging mass cytometry. Sci Immunol. 2022; 7: eabi5072. doi:10.1126/sciimmunol.abi5072.
154. Xu Y, Wang X, Li Y, Mao Y, Su Y, Mao Y, et al. Multimodal single cell-resolved spatial proteomics reveal pancreatic tumor heterogeneity. Nat Commun. 2024; 15: 10100. doi:10.1038/s41467-024-54438-0.
155. Li Z, Li Y, Xiang J, Wang X, Yang S, Zhang X, et al. AI-enabled virtual spatial proteomics from histopathology for interpretable biomarker discovery in lung cancer. Nat Med. 2026; 32: 231–44. doi:10.1038/s41591-025-04060-4.
156. Oren Y, Tsabar M, Cuoco MS, Amir-Zilberstein L, Cabanos HF, Hütter JC, et al. Cycling cancer persister cells arise from lineages with distinct programs. Nature. 2021; 596: 576–82. doi:10.1038/s41586-021-03796-6.
157. Philip M, Fairchild L, Sun L, Horste EL, Camara S, Shakiba M, et al. Chromatin states define tumour-specific T cell dysfunction and reprogramming. Nature. 2017; 545: 452–6. doi:10.1038/nature22367.
158. Long GV, Dummer R, Hamid O, Gajewski TF, Caglevic C, Dalle S, et al. Epacadostat plus pembrolizumab versus placebo plus pembrolizumab in patients with unresectable or metastatic melanoma (ECHO-301/KEYNOTE-252): a phase 3, randomised, double-blind study. Lancet Oncol. 2019; 20: 1083–97. doi:10.1016/s1470-2045(19)30274-8.
159. Bendell J, LoRusso P, Overman M, Noonan AM, Kim D-W, Strickler JH, et al. First-in-human study of oleclumab, a potent, selective anti-CD73 monoclonal antibody, alone or in combination with durvalumab in patients with advanced solid tumors. Cancer Immunol Immunother. 2023; 72: 2443–58. doi:10.1007/s00262-023-03430-6.
160. Aggarwal C, Martinez-Marti A, Majem M, Barlesi F, Carcereny E, Chu Q, et al. Durvalumab Alone or Combined With Novel Agents for Unresectable Stage III Non-Small Cell Lung Cancer: Update From the COAST Randomized Clinical Trial. JAMA Netw Open. 2025; 8: e2518440. doi:10.1001/jamanetworkopen.2025.18440.
161. Barlesi F, Cho BC, Goldberg SB, Yoh K, Zimmer Gelatti AC, Mann H, et al. PACIFIC-9: Phase III trial of durvalumab + oleclumab or monalizumab in unresectable stage III non-small-cell lung cancer. Future Oncol. 2024; 20: 2137–47. doi:10.1080/14796694.2024.2354160.
162. Segal NH, Tie J, Kopetz S, Ducreux M, Chen E, Dienstmann R, et al. COLUMBIA-1: a randomised study of durvalumab plus oleclumab in combination with chemotherapy and bevacizumab in metastatic microsatellite-stable colorectal cancer. Br J Cancer. 2024; 131: 1005–13. doi:10.1038/s41416-024-02796-3.
163. Altman DG, McShane LM, Sauerbrei W, Taube SE. Reporting Recommendations for Tumor Marker Prognostic Studies (REMARK): explanation and elaboration. PLoS Med. 2012; 9: e1001216. doi:10.1371/journal.pmed.1001216.
164. Simon RM, Paik S, Hayes DF. Use of archived specimens in evaluation of prognostic and predictive biomarkers. J Natl Cancer Inst. 2009; 101: 1446–1452. doi:10.1093/jnci/djp335.
165. US Food and Drug Administration. Biomarker qualification: evidentiary framework. Draft guidance for industry and FDA staff. Silver Spring, MD: US Food and Drug Administration; 2018.
166. US Food and Drug Administration. In vitro companion diagnostic devices. Guidance for industry and Food and Drug Administration staff. Silver Spring, MD: US Food and Drug Administration; 2014.
167. Ma J, Tang L, Tan Y, Xiao J, Wei K, Zhang X, et al. Lithium carbonate revitalizes tumor-reactive CD8+ T cells by shunting lactic acid into mitochondria. Nat Immunol. 2024; 25: 552–61. doi:10.1038/s41590-023-01738-0.
168. US Food and Drug Administration. Lithium and lithium carbonate prescribing information. Reference ID 4366479. Silver Spring, MD: US Food and Drug Administration; 2018.
169. Chi JJ, Xie P, Cheng MH, Zhu Y, Cui X, Watson J, et al. MGAT1-guided complex N-glycans on CD73 regulate immune evasion in triple-negative breast cancer. Nat Commun. 2025; 16: 3552. doi:10.1038/s41467-025-58524-9.
170. Zhu Y, Banerjee A, Xie P, Ivanov AA, Uddin A, Jiao Q, et al. Pharmacological suppression of the OTUD4/CD73 proteolytic axis revives antitumor immunity against immune-suppressive breast cancers. J Clin Invest. 2024; 134: e176390. doi:10.1172/jci176390.

171. Wang Y, Chai Y, Liu Y, Liu X, Zhang Y, Yang Z, et al. Inhibition of tumor cell macropinocytosis driver DHODH reverses immunosuppression and overcomes anti-PD1 resistance. Immunity. 2025; 58: 2456-2471.e6. doi:10.1016/j.immuni.2025.07.013.
172. Liu Y, Liang G, Xu H, Dong W, Dong Z, Qiu Z, et al. Tumors exploit FTO-mediated regulation of glycolytic metabolism to evade immune surveillance. Cell Metab. 2021; 33: 1221-1233.e11. doi:10.1016/j.cmet.2021.04.001.
173. Mortazavi Farsani SS, Soni J, Jin L, Yadav AK, Bansal S, Mi T, et al. Pyruvate kinase M2 activation reprograms mitochondria in CD8 T cells, enhancing effector functions and efficacy of anti-PD1 therapy. Cell Metab. 2025; 37: 1294-1310.e7. doi:10.1016/j.cmet.2025.03.003.
174. Ma S, Ong L-T, Jiang Z, Lee WC, Lee PL, Yusuf M, et al. Targeting P4HA1 promotes CD8+ T cell progenitor expansion toward immune memory and systemic anti-tumor immunity. Cancer Cell. 2025; 43: 213-231.e9. doi:10.1016/j.ccell.2024.12.001.
175. Krishna S, Lowery FJ, Copeland AR, Bahadiroglu E, Mukherjee R, Jia L, et al. Stem-like CD8 T cells mediate response of adoptive cell immunotherapy against human cancer. Science. 2020; 370: 1328–34. doi:10.1126/science.abb9847.
176. Liu S, Guruprasad P, Ramasubramanian R, Madhu B, Paruzzo L, Han K, et al. β-hydroxybutyrate enhances the metabolic fitness of CAR T cells in cancer. Cell. 2026; 189: 1701-1716.e24. doi:10.1016/j.cell.2026.02.004.
177. Hope HC, de Sostoa J, Ginefra P, Andreatta M, Chiang Y-H, Ronet C, et al. Age-associated nicotinamide adenine dinucleotide decline drives CAR-T cell failure. Nat Cancer. 2025; 6: 1524–36. doi:10.1038/s43018-025-00982-7.
178. Si X, Shao M, Teng X, Huang Y, Meng Y, Wu L, et al. Mitochondrial isocitrate dehydrogenase impedes CAR T cell function by restraining antioxidant metabolism and histone acetylation. Cell Metab. 2024; 36: 176-192.e10. doi:10.1016/j.cmet.2023.12.010.
179. Jackson CM, Pant A, Dinalankara W, Choi J, Jain A, Nitta R, et al. The cytokine meteorin-like inhibits anti-tumor CD8+ T cell responses by disrupting mitochondrial function. Immunity. 2024; 57: 1864-1877.e9. doi:10.1016/j.immuni.2024.07.003.
180. Niu C, Wei H, Pan X, Wang Y, Song H, Li C, et al. Foxp3 confers long-term efficacy of chimeric antigen receptor-T cells via metabolic reprogramming. Cell Metab. 2025; 37: 1426-1441.e7. doi:10.1016/j.cmet.2025.04.008.
181. Ravi VM, Will P, Kueckelhaus J, Sun N, Joseph K, Salié H, et al. Spatially resolved multi-omics deciphers bidirectional tumor-host interdependence in glioblastoma. Cancer Cell. 2022; 40: 639-655.e13. doi:10.1016/j.ccell.2022.05.009.